LITHOS 414–415 (2022) 106622

Contents lists available at ScienceDirect

LITHOS

journal homepage: www.elsevier.com/locate/lithos

Pre-Late Eocene position of the Lüchun-Jinping microblock in western Yangtze Craton: Constraints from Eocene-Oligocene lamprophyres in southeastern Tibet

Yang Shen [a,b], Yuan-Chuan Zheng [a,*], Zeng-Qian Hou [c], Jan Marten Huizenga [d,e,f], Ai-Ping Zhang [g], Zi-Xuan Wang [a], Xin Li [a], Pei-Yan Xu [h], Chang-Da Wu [c], Si-Qi Liu [a]

[a] State Key Laboratory of Geological Processes and Mineral Resources, and School of Earth Sciences and Resources, China University of Geosciences, Beijing 100083, China
[b] Institute für Geowissenschaften, Johannes Gutenberg Universität, Mainz, 55099, Germany
[c] Institute of Geology, Chinese Academy of Geological Sciences, Beijing 100037, China
[d] Faculty of Environmental Sciences and Natural Resource Management, Norwegian University of Life Sciences, P.O. Box 5003, NO-1432, Ås, Norway
[e] Economic Geology Research Institute (EGRU), College of Science and Engineering, James Cook University, Townsville, Queensland 4811, Australia
[f] Department of Geology, University of Johannesburg, PO, 524, Auckland Park, 2006, South Africa
[g] School of Earth Sciences, Yunnan University, Kunming 650500, China
[h] Chengdu Center, China Geological Survey, Chengdu, 610081, China

ARTICLE INFO

Keywords:
Lamprophyres
Geochemistry
Lithospheric mantle
Paleoposition
Lüchun-Jinping microblock
Southeastern Tibet

ABSTRACT

The tectono-magmatic history of the Lüchun-Jinping microblock and its possible affinity with the Yangtze Craton are important elements for the reconstruction of Cenozoic plate tectonics in southeastern Tibet. In order to constrain the affinity and decipher the pre-Cenozoic paleopositon of the Lüchun-Jinping microblock, we focused on the petrogenesis of Eocene-Oligocene lamprophyres in the Lüchun-Jinping microblock. The lamprophyres yield zircon U—Pb ages of 34.7–33.3 Ma and exhibit potassic-ultrapotassic features with elevated K_2O/Na_2O (1.4–4.0) ratios. They are characterized by high concentrations of compatible elements (e.g., Cr = 187–692 ppm, Ni = 31–218 ppm), large-ion-lithophile elements and light rare-earth elements enrichment, high-field-strength elements depletion, and high radiogenic isotopic values, i.e. $(^{87}Sr/^{86}Sr)_i$ = 0.7063–0.7078 and εNd(t) = −3.9 to −2.4. Combined with the low Nb/U ratios, these features suggest that the lithospheric mantle source was metasomatized by subduction-related fluids beneath the Lüchun-Jinping microblock. The relatively high Rb/Sr ratios and high heavy rare-earth element contents indicate that these lamprophyres were derived from partial melting of a phlogopite-bearing lherzolite within the spinel stability field. The parental magmas have experienced fractional crystallization of olivine and clinopyroxene during emplacement. Comprehensive comparisons between the lamprophyres from the Lüchun-Jinping microblock and the potassic-ultrapotassic mafic rocks from the western Yangtze Craton indicate that the Lüchun-Jinping microblock can be regarded as a dismembered part of the western Yangtze Craton due to continental extrusion and Cenozoic sinistral displacement. The compositional trends of the potassic-ultrapotassic mafic rocks suggest that the palaeogeographic position of the Lüchun-Jinping microblock was near the Dali area (west of the Binchuan) and close to the Jinshajiang suture zone before the Cenozoic.

1. Introduction

Most fragmental blocks in southeastern Asia have witnessed the subduction and closure of different branches of the Paleo-Tethyan oceans in the Permo-Triassic (Deng et al., 2014; Faure et al., 2014; Metcalfe, 2013). The Ailaoshan ocean, one branch of the Paleo-Tethyan ocean, was consumed, which led to Late Permian amalgamation of the Simao-Indochina block with the Yangtze Craton (Metcalfe, 2013). However, the exact location of the Late Permian collisional suture between the Simao-Indochina and the Yangtze Craton is still controversial.

* Corresponding author at: School of Earth Sciences and Resources, China University of Geosciences, 29# Xue-Yuan Road, Haidian District, Beijing, 100083, P. R. China.
E-mail address: zhengyuanchuan@gmail.com (Y.-C. Zheng).

https://doi.org/10.1016/j.lithos.2022.106622
Received 5 October 2021; Received in revised form 11 January 2022; Accepted 6 February 2022
Available online 10 February 2022

On the one hand, the Cenozoic Ailaoshan shear zone has been regarded as the location of this suture (Leloup et al., 1995; Sone and Metcalfe, 2008) mainly because the northern part of the shear zone merges with the "ophiolite belt", which was formed as a result of the closure of the Ailaoshan ocean (Leloup et al., 1995; Fig. 1c). On the other hand, some researchers have suggested that the collisional suture is located >50 km to the west of Ailaoshan shear zone, which is based on the distribution of picritic flows in the Jinping area belonging to the Emeishan flood basalts (Chung et al., 1997; Xiao et al., 2003; Fig. 1c). The location of the suture proposed by Chung et al. (1997) takes into account that the sinistral offset of the Ailaoshan shear zone was ~600 km in the Cenozoic due to continental extrusion (Leloup et al., 1995; Tapponnier et al., 1990). The two different locations proposed for the same collisional suture have resulted in the existence of a suspect microblock, namely the Lüchun-Jinping microblock, which is situated between the two proposed suture localities. The affinity of this Lüchun-Jinping microblock remains a matter of debate. The former location of the suture (Leloup et al., 1995; Sone and Metcalfe, 2008) implies that the Lüchun-Jinping microblock is part of the Simao-Indochina block. On the other hand, the latter proposal of the collisional suture (Chung et al., 1997; Faure et al., 2014) indicates that the Lüchun-Jinping microblock is a cratonic fragment belonging to the Yangtze Craton. However, its relative paleoposition is ambiguous due to the Oligocene sinistral movement along the Ailaoshan-Red River shear zone (Leloup et al., 1995; Liu et al., 2020; Tapponnier et al., 1990).

In the Cenozoic, the Indian continent collided with the Eurasian

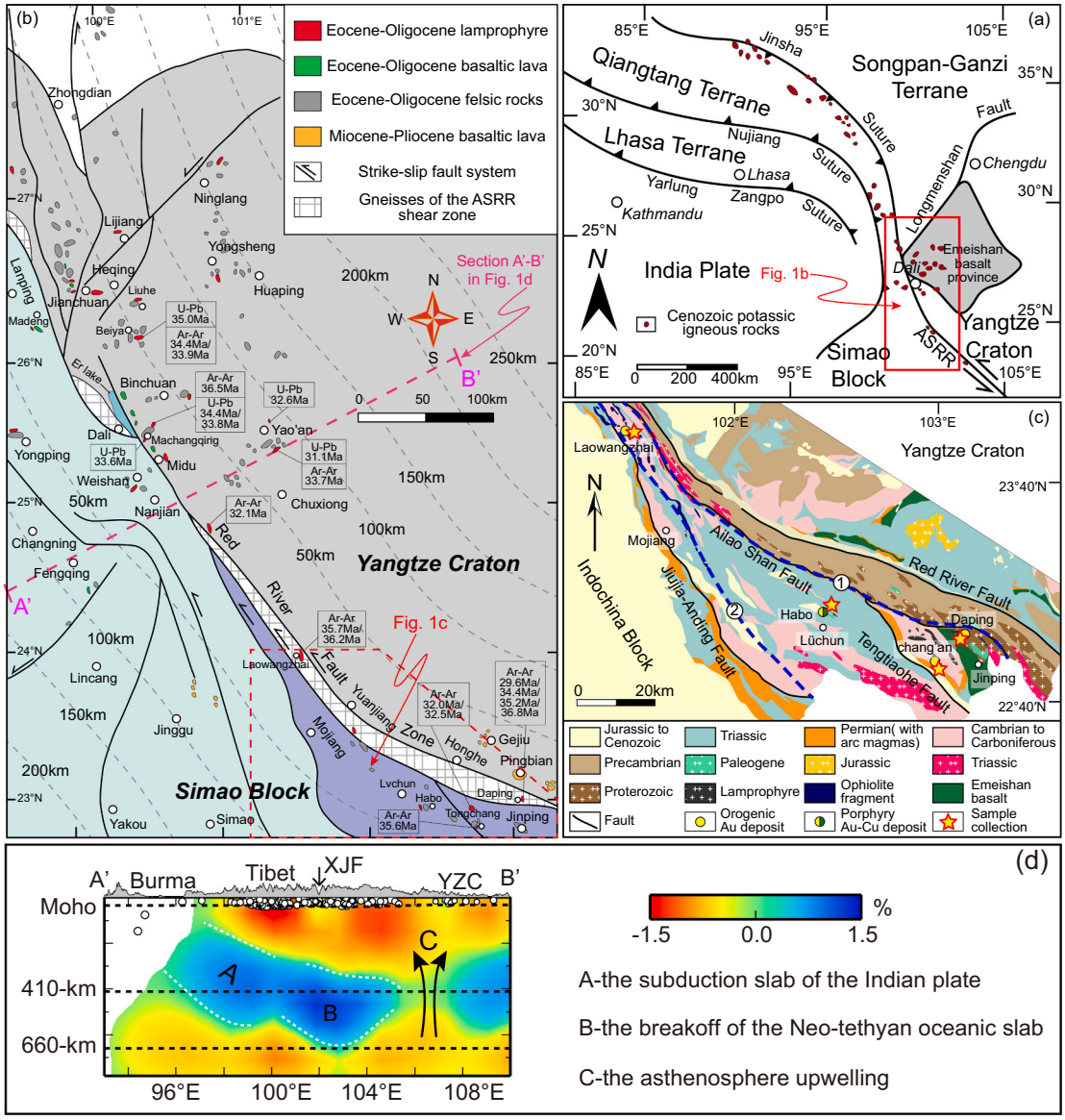

Fig. 1. (a) Tectonic framework of Tibetan Plateau and surrounding areas, the red fields denote Cenozoic potassic igneous rocks along Jinshajiang-Ailaoshan Suture (modified from Xu et al., 2001). (b) Simplified geological map of the western Yangtze Craton and Simon Block (see Table S1 for cited ages), showing the distribution of Eocene-Oligocene potassic magmatic rocks (modified from Lu et al., 2012). (c) Regional geological map of the Ailaoshan tectonic belt showing the stratigraphic, structural and igneous components, and the sample locations of lamprophyres in Lüchun-Jinping microblock (modified after Wang et al., 2014). The locations of the suture between Yangtze Craton and Simao-Indochina block numbered 1 and 2 are from Sone and Metcalfe (2008) and Chung et al. (1997), respectively. (d) Vertical cross section of P-wave tomography along the profile A'-B′ shown on the geologic map of southeastern Tibet (modified from Lei and Zhao, 2016). The red and blue colors denote low-V and high-V anomalies, respectively. The velocity perturbation scale (in %) is shown on the right. The white dots show seismicity within a width of 50 km of each profile. The three dashed lines denote the Moho, 410 and 660 km discontinuities. The surface topography is shown above the cross section. The arrows denote locations of active faults. XJF = Xiaojiang fault; YZC = Yangtze Craton. (For interpretation of the references to colour in this figure legend, the reader is referred to the web version of this article.)

continent, forming prominent NW-SE trending strike-slip faults and the Ailaoshan-Red River shear zone in southeastern Tibet (Chung et al., 2005; Hou et al., 2007; Fig. 1a, b). Numerous post-collisional magmatic rocks were widely developed along the Jinshajiang-Ailaoshan shear zone on both sides and form a semi-continuous potassic magmatic province in southeastern Tibet (Fig. 1; Wang et al., 2001; Chung et al., 2005; Lu et al., 2012) and also in the Lüchun-Jinping microblock (Fig. 1b, c). The post-collisional magmatic rocks include intermediate to felsic shoshonitic syenites and adakitic granitoids (Lu et al., 2012; Shen et al., 2021; Wang et al., 2001), and potassic-ultrapotassic mafic rocks (Guo et al., 2005; Huang et al., 2010; Yu et al., 2020). The majority of the mafic rocks in the Lüchun-Jinping microblock (Chen et al., 2014; Li et al., 2019; Yu et al., 2020) include hypabyssal dykes with mafic phenocrysts. They are referred to as potassic-ultrapotassic lamprophyres with high MgO and K_2O contents, and elevated K_2O/Na_2O ratios (Foley et al., 1987; Rock, 1987). Lamprophyres are considered to be primary mantle-derived magmas (Foley et al., 1987) produced by a low degree melting of metasomatized sub-continental lithospheric mantle (SCLM) (Conticelli et al., 2009; Foley, 1992). They are well known to be spatially associated with certain types of economic gold-(copper) deposits (Müller and Groves, 2000). Regardless of their small volumes and petrological peculiarities, lamprophyres are refractory relative to the intermediate-felsic crustal-derived rocks, and they are natural lithoprobes of the SCLM providing insights into the evolution of the continental lithosphere (Foley et al., 1987; Prelević et al., 2012). Therefore, the potassic-ultrapotassic lamprophyres can reveal the nature and evolution of lithospheric mantle beneath the Lüchun-Jinping microblock, and provide new insights into the affinity and paleogeographic location of the Lüchun-Jinping microblock.

In this contribution, the Eocene-Oligocene potassic-ultrapotassic lamprophyres from the Lüchun-Jinping microblock were investigated with respect to zircon U—Pb geochronology, whole-rock major and trace element, and Sr-Nd-Pb isotope geochemistry. The objectives of this study are to: (1) determine the petrogenesis of the lamprophyres; (2) trace the intrinsic information about the nature and evolution of their mantle sources; (3) constrain the affinity and decipher the pre-Cenozoic paleogeographic location of the Lüchun-Jinping microblock.

2. Geological setting and petrography

2.1. Geological background

The structural framework of southeastern Tibet was formed as a result of the Paleo-Tethyan ocean closure and the subsequent amalgamation of Gondwana-derived micro-continental blocks and the Paleozoic arc terranes (Cocks and Torsvik, 2013). The continental blocks in the southeastern Tibet, including the Simao-Indochina, Yangtze Craton and East Qiangtang, were amalgamated after the Paleo-Tethyan oceans were consumed by Permian-Triassic oceanic subduction (Metcalfe, 2013). The Cenozoic evolution of the southeastern Tibet was largely controlled by the India-Eurasia collision (Deng et al., 2014).

The Simao-Indochina block is separated from the Baoshan and Yangtze Craton by the Changning-Menglian and Ailaoshan sutures (Fig. 1b), respectively, which were formed by the closures of the Paleo-Tethyan ocean and its branches (Metcalfe, 2013). The basement of the Simao terrane is exposed along the Jinshajiang-Ailaoshan ranges and consists of Precambrian high-grade metamorphic rocks (Zhong, 2000). It is overlain by a thick sequence of Paleozoic-Mesozoic low-grade metasedimentary rocks (Pan et al., 2003). The Simao block represents the northern extension of the Indochina block considering the two Paleozoic sutures along its eastern and western margins (Metcalfe, 2013). The Yaxuanqiao-Wusu arc comprises Late Carboniferous to Late Permian (300–255 Ma) mafic to intermediate magmatic rocks and developed at the eastern margin of the Simao block (Fig. 1c; Fan et al., 2010). Late Permian arc-like magmatic rocks occur east of the Triassic Lincang batholith in Yunxian-Jinggu arc (western margin of Simao block) (Hennig et al., 2009). The Yangtze Craton was situated near the periphery of the Rodinia supercontinent since the Neoproterozoic (Zhou et al., 2006) and on the site of Mozambique oceanic subduction during the Neoproterozoic (1000–740 Ma; Zhou et al., 2006; Zhao and Zhou, 2007; Sun et al., 2009). It is composed of an Archean-Neoproterozoic crystalline basement and a Late Neoproterozoic-Cenozoic cover sequence (Zhou et al., 2006). Along the western and northern edges of the craton, numerous remnants of Neoproterozoic (1000–740 Ma) volcanic rocks and plutons with arc-like geochemical features are present. They represent the Neoproterozoic Panxi-Hannan magmatic arc (Zhao and Zhou, 2007; Zhou et al., 2006), which are unconformably overlain by Late Neoproterozoic-Cretaceous strata (Zhou et al., 2006). The cover strata comprise Silurian-Triassic clastic-carbonate sequences and Late Permian (260–250 Ma) Emeishan continental flood basalt (Chung et al., 1997; Xiao et al., 2003).

The wedge-shaped Lüchun-Jinping microblock is located in the southern segment of the Ailaoshan tectonic belt (southeastern Tibet) bounded by the Jiujia-Anding fault in the west and the Ailaoshan-Red River shear zone in the east (Wang et al., 2014; Faure et al., 2016; Fig. 1c). In the eastern part, Neoproterozoic meta-volcanic and metasedimentary rocks including gneiss, amphibolite, and schist crop out (Cai et al., 2014; Wang et al., 2016). The Neoproterozoic amphibolites show an arc-like geochemistry, including pronounced Nb-Ta-Ti depletion and whole-rock εNd(t) values ranging from −3.5 to −2.0 (Cai et al., 2014), indicating that the belt was part of the Panxi-Hannan arc surrounding the western to northern margin of the Yangtze Craton. In the western part, the ophiolitic complex of the Paleo-Tethyan ocean, Paleozoic to Mesozoic sedimentary rocks, and Paleo-Tethyan subduction-related Permian igneous rocks with positive εNd(t) ranging from +3.5 to +5.5, extending from Yaxuanqiao to Lvchun, occur (Fan et al., 2010). In addition, Permian basaltic lavas (including volcanic breccias, basaltic tuffs, and massive basalt flows) are widespread forming a narrow (≤20 km), NW-SE trending belt of >350 km long in the Jinping district (Fig. 1c; Xiao et al., 2003; Wang et al., 2007).

Cenozoic potassic magmas associated with the Indian-Asian collision are widespread in southeastern Tibet (Fig. 1; Chung et al., 1998; Wang et al., 2001; Lu et al., 2012). Together with the coeval mafic to felsic magmas in the Qiangtang terrane, these magmas form an arc-like Eocene-Oligocene (43–32 Ma) belt extending over 2000 km along the translithospheric Jinshajiang-Ailaoshan suture zone (Fig. 1a; Chung et al., 2005). In the Ailaoshan tectonic belt, the Eocene-Oligocene potassic igneous rocks include felsic and mafic rocks (Fig. 1c). The felsic intrusions consist of syenite, granite, and quartz monzonite with zircon U—Pb ages ranging between 36.3 and 33.7 Ma (Xin et al., 2020; Xu et al., 2012; Zhu et al., 2013). The widely exposed mafic units are dominated by lamprophyre dykes, with minor mafic lavas. The lamprophyres yield phlogopite $^{40}Ar/^{39}Ar$ ages of 36.8–29.6 Ma (Supplementary Table S1; Wang et al., 2001; Chen et al., 2014), and are spatially associated with the economic gold-copper deposits (Fig. 1c; Yu et al., 2020).

2.2. Sample descriptions

Sixteen least-altered lamprophyre samples were collected from the Laowangzhai, Habo, Daping and Chang'an ore districts in the Lüchun-Jinping microblock (Fig. 1c). These grayish-black lamprophyres occur as NE and NW trending dykes, with a width of 1–5 m and a length of 5–30 m (Fig. 2a). The lamprophyre dykes in Chang'an gold district are related to the potassic felsic intrusions and turbidites (Fig. 2a; Yu et al., 2020). The Daping lamprophyre dykes occur (sub-)parallel to the auriferous quartz veins, hosted in the limestones (Chen et al., 2014). The Laowangzhai lamprophyres are mainly intruded in the carbonaceous slates and occur along the subsidiary faults (Li et al., 2019). The lamprophyre dykes in the Habo ore district are hosted in the felsic granite bodies and the surrounding country rocks (Zhu et al., 2013). The lamprophyres from the Habo district are amphibole-dominated plagioclase-bearing

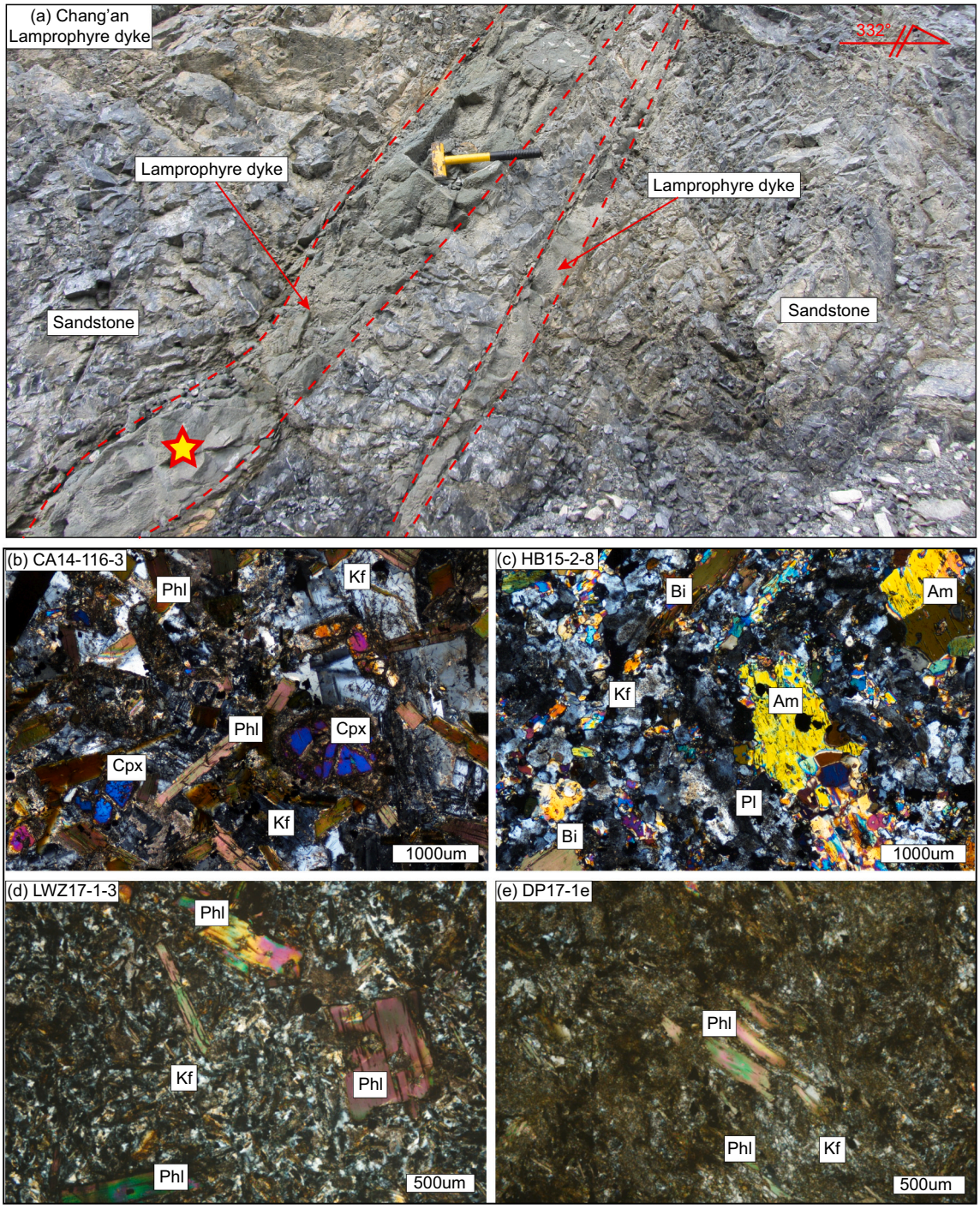

Fig. 2. Field photograph and microphotographs illustrating mineralogical and textural features of lamprophyres from the Lüchun-Jinping microblock. (a) Field photograph of lamprophyre dyke from the Chang'an ore district. (b) Photomicrograph of lamprophyres from the Chang'an ore district. Sample CA14–116-3 of fresh phlogopite and clinopyroxene phenocrysts in a fresh groundmass dominated by K-feldspar (crossed polarized light). (c) Photomicrograph of lamprophyres from the Habo ore district. Sample HB15–2-8 of fresh biotite and amphibole phenocrysts in a fresh groundmass dominated by plagioclase and K-feldspar (crossed polarized light). (d) and (e) Photomicrographs (samples LWZ17–1-3 and DP17–1e) of lamprophyres from the Laowangzhai and Daping ore districts, respectively, showing fresh phlogopite phenocrysts in the relatively fresh groundmass of clinopyroxene, phlogopite and feldspar (crossed polarized light). Abbreviations: Kfs = K-feldspar; Phl = phlogopite; Bi = biotite; Am = amphibole; Cpx = clinopyroxene.

kersantites (Fig. 2c), whereas all the other sampled lamprophyres are phlogopite-dominated plagioclase-free minettes (Fig. 2b, d, e; Table 1; Le Maitre, 2002). For simplicity, we refer to them as lamprophyres hereafter. The lamprophyres display predominantly (micro-) porphyritic textures (Fig. 2b-e), with phenocrysts including eu- to subhedral phlogopite, biotite, and clinopyroxene or amphibole. The groundmass consists of anhedral phlogopite, biotite, K-feldspar, plagioclase and clinopyroxene or amphibole (Table 1; Fig. 2b-e). Accessory minerals include Fe—Ti oxides, zircon, titanite, and apatite. A summary including sample locations and brief description of the lamprophyres is provided in Table 1.

Table 1
Phenocryst and groundmass mineral assemblages of the potassic-ultrapotassic lamprophyres from the Lüchun-Jinping microblock, southeastern Tibet.

Sample	Locality	Longitude (°E)	Latitude (°N)	Age (Ma)	Mg#	Rock type	Phenocrysts (vol%)	Groundmass
CA14–116-1	Chang'an	103.036	22.811	34.7 ± 0.44	77	Tephrite	Phl(10) + Cpx(3)	Phl + Cpx + San + Fe-Ti
CA14–116-2	Chang'an	103.036	22.811		74	Potassic trachybasalt	Phl(8) + Cpx(5)	Phl + Cpx + San + Ap + Fe-Ti
CA14–116-3	Chang'an	103.036	22.811		79	Potassic trachybasalt	Phl(7) + Cpx(5)	Phl + Cpx + San + Fe-Ti
CA14–116-5	Chang'an	103.036	22.811		78	Potassic trachybasalt	Phl(10) + Cpx(3)	Phl + Cpx + San + Ap + Fe-Ti
CA1709–3	Chang'an	103.036	22.810		74	Tephrite	Phl + Cpx	Phl + Cpx + San + Fe-Ti
CA1710-3a	Chang'an	103.036	22.810		73	Tephrite	Phl + Cpx	Phl + Cpx + San + Fe-Ti
CA1711–1	Chang'an	103.036	22.810		75	Tephrite	Phl + Cpx	Phl + Cpx + San + Fe-Ti
HB15–2-8	Habo	102.550	22.956		69	Latite	Am(3) + Bi(7)	Am+Bi+Pl + San + Fe-Ti
HB15–2-9	Habo	102.550	22.956		68	Latite	Am+Bi	Am+Bi+Pl + San + Ap + Fe-Ti
HB15–2-10	Habo	102.550	22.956		68	Latite	Am+Bi	Am+Bi+Pl + San + Fe-Ti
LWZ1701–1	Laowangzhai	101.459	23.897	34.6 ± 0.29	69	Potassic trachybasalt	Phl(5) + Cpx(1)	Phl + Cpx + San + Fe-Ti
LWZ1701–3	Laowangzhai	101.459	23.897		68	Shoshonite	Phl(5)	Phl + San + Fe-Ti
LWZ1701–5	Laowangzhai	101.459	23.897		69	Shoshonite	Phl(6)	Phl + San + Ap + Fe-Ti
DP17–1a	Daping	103.090	22.894	33.3 ± 0.34	68	Shoshonite	Phl(5)	Phl + San + Ap + Fe-Ti
DP17–1e	Daping	103.090	22.894		66	Latite	Phl(3)	Phl + San + Fe-Ti
DP-93	Daping	103.090	22.894		69	Shoshonite	Phl(5)	Phl + San + Fe-Ti

Mg# = MgO/(MgO + FeOT) in atomic ratio. Proportions in percent of phenocrysts are shown in parentheses (vol%). Am = amphibole; Ap = apatite; Cpx = clinopyroxene; Fe-Ti = Fe-Ti oxides; Phl = phlogopite; Pl = plagioclase; San = sanidine.

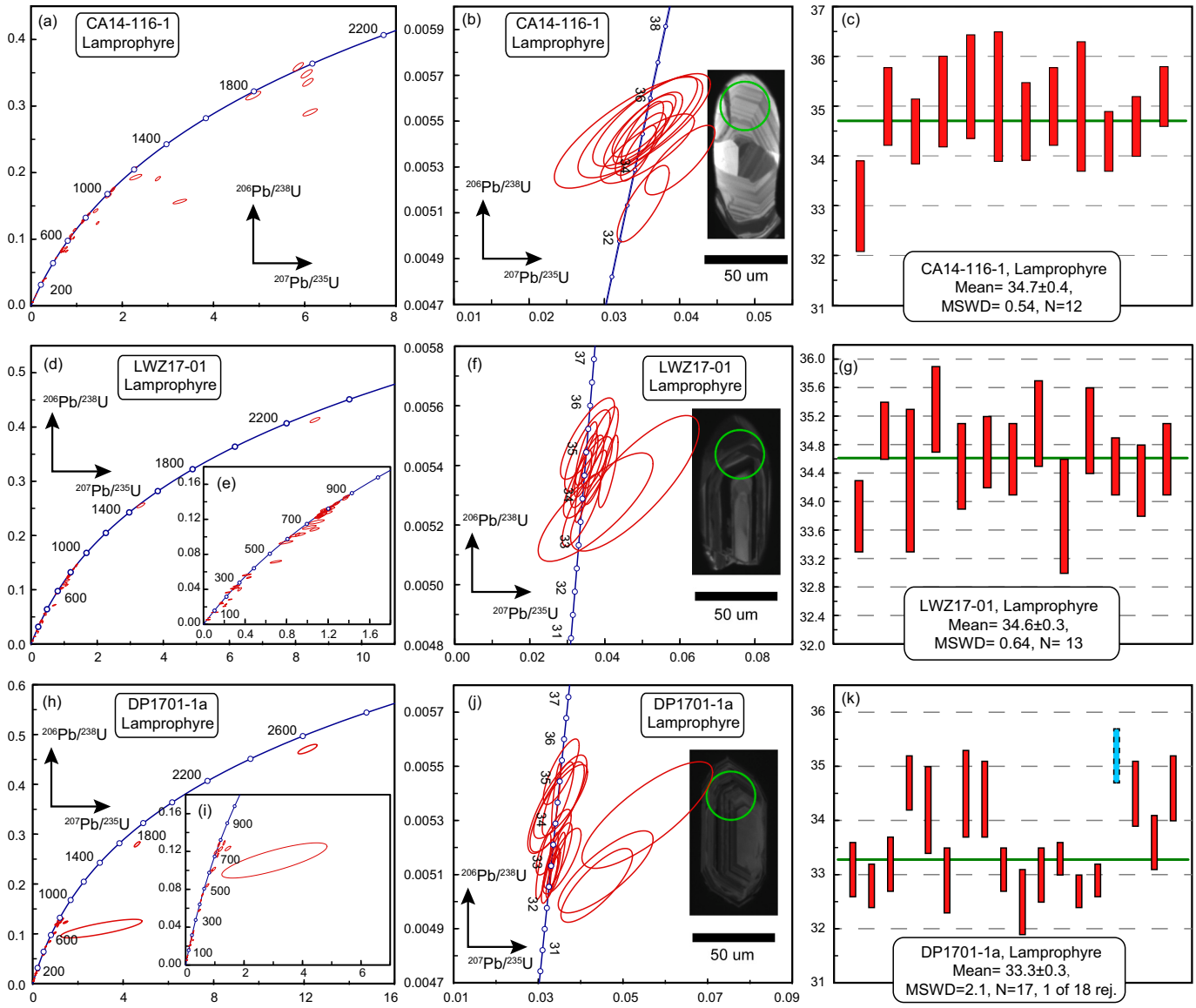

Fig. 3. Zircon U—Pb concordia diagrams and CL images for representative zircon grains of studied lamprophyres in the Lüchun-Jinping microblock. (a-c) Chang'an lamprophyre (CA14–116-1), (d-g) Laowangzhai lamprophyre (LWZ17–01), (h-k) Daping lamprophyre (DP1701–1a). Solid green circles indicate the locations of U—Pb analysis. (For interpretation of the references to colour in this figure legend, the reader is referred to the web version of this article.)

3. Analytical methods

Zircons Laser Ablation Inductively Coupled Plasma Mass Spectrometry (LA–ICP–MS) U—Pb geochronology were conducted for three samples collected from the Laowangzhai, Daping and Chang'an gold deposits. Measurements of U, Th and Pb isotopes were conducted using the LA–ICP–MS at the Geologic Lab Centre at the China University of Geosciences (Beijing). The instrument couples a quadrupole ICP–MS (Agilient 7500a) and an UP-193 Solid-State laser (193 nm, New Wave Research Inc.) with the automatic positioning system. Major and trace element analyses were determined for all sixteen samples at the Wuhan SampleSolution Analytical Technology Co., Ltd., Wuhan, using the Rigaku Primus II X-ray fluorescence (XRF) and the Agilent 7700e inductively coupled plasma-mass spectrometry (ICP–MS) system, respectively. Sr–Nd–Pb isotopic analyses were obtained from eight representative lamprophyre samples, and isotopic ratios were measured using a Finnigan MAT-262 thermal ionisation mass spectrometer at the Laboratory for Radiogenic Isotope Geochemistry, University of Science and Technology of China. Detailed analytical methods are given in Supplementary Text S1. All analytical results and analyses of standards are listed in Supplementary Table S2–S3.

4. Results

4.1. Zircon U—Pb geochronology

To constrain the timing of the onset and duration of crystallization of lamprophyres in the Lüchun-Jinping microblock, the LA-ICP-MS U—Pb analytical work focuses on the zircons from the Chang'an, Laowangzhai and Daping lamprophyres. The zircon grains from these lamprophyrees are elongated to stubby in shape, with average crystal lengths of 50–200 μm and length-to-width ratios ranging from 1:1 to 3:1. These zircons show weak magmatic oscillatory zoning, with some of the zircon grains not showing any oscillatory zoning at all (Fig. S1). Just a few zircons show oscillatory and planar zoning in the rims of the crystals (Fig. 3; Fig. S1). All the U—Pb dating results are listed in Table S2, and presented on concordia diagrams (Fig. 3).

Fifty spot analyses carried out on zircons from the Chang'an lamprophyre (CA14–116-1) yielded Th/U ratios varying from 0.08 to 2.51 with only one grain having Th/U ratio < 0.1. The fifty analyses show a considerable spread of the $^{206}Pb/^{238}U$ and $^{207}Pb/^{235}U$ ratios on the U—Pb concordia diagram, considerable spread in $^{206}Pb/^{238}U$ and $^{207}Pb/^{235}U$ ratios can be observed (Fig. 3a), with $^{206}Pb/^{238}U$ ages ranging from 1977 to 33.0 Ma (Table S2). The twelve youngest analyses yield $^{206}Pb/^{238}U$ concordant ages of 35.4–33.0 Ma, with a weighted-mean age of 34.7 ± 0.4 Ma (1σ, MSWD = 0.5) (Fig. 3b, c). In addition, there are a large amount of inherited zircon ages, with four age populations at the Proterozoic (1977–605 Ma, n = 23), Cambrian (537–502 Ma, n = 7), Permian-Triassic (258–232 Ma, n = 3), and Cretaceous (112–67 Ma, n = 4) (Table S2; Fig. 3a).

Fifty-six spot analyses carried out on zircons from the Laowangzhai lamprophyre (LWZ1701–1) yielded Th/U ratios of 0.07–2.94 with only one grain having Th/U ratio < 0.1. A considerable spread of $^{206}Pb/^{238}U$ and $^{207}Pb/^{235}U$ ratios can be observed on the concordia diagram (Fig. 3d), with $^{206}Pb/^{238}U$ ages ranging from 2228 to 33.8 Ma (Table S2). The thirteen youngest analyses yield $^{206}Pb/^{238}U$ concordant ages of 35.3–33.8 Ma, with a weighted-mean age of 34.6 ± 0.3 Ma (1σ, MSWD = 0.6) (Fig. 3f, g). There are also numerous inherited zircon ages defining three age populations, i.e. at the Neoproterozoic (877–577 Ma, n = 24), Permian-Triassic (276–231 Ma, n = 5), and Jurassic-Cretaceous (181–88 Ma, n = 7) (Table S2; Fig. 3e).

Fifty-three spot analyses carried out on zircons from the Daping lamprophyre (DP17–1a) yield Th/U ratios varying from 0.11 to 2.38. Again, a considerable spread of $^{206}Pb/^{238}U$ and $^{207}Pb/^{235}U$ ratios on the concordia diagram can be observed (Fig. 3h), with $^{206}Pb/^{238}U$ ages ranging from 2487 to 32.5 Ma (Table S2). The eighteen youngest analyses yield concordant $^{206}Pb/^{238}U$ ages of 35.2–32.5 Ma, with a weighted-mean age of 33.3 ± 0.3 Ma (1σ, MSWD = 2.1) (Fig. 3j, k). There are also abundant inherited zircon ages defining four age populations at the Proterozoic (2487–606 Ma, n = 11), Triassic (272–209 Ma, n = 4), Jurassic-Cretaceous (191–110 Ma, n = 10) and Paleocene-Eocene (65–48 Ma, n = 5) (Table S2; Fig. 3h).

4.2. Whole-rock major and trace element

The SiO_2 (46.1–56.7 wt%) and MgO (6.0–13.5 wt%) contents of the lamprophyres from the Lüchun-Jinping microblock show a wide range (Table S3). All lamprophyre samples are part of the alkaline series, ranging from tephrite, potassic trachybasalt to shoshonite and latite in the total alkalis-silica (TAS) diagram (Fig. 4a, Le Maitre, 2002). The lamprophyres belong to the calc-alkaline series according to Rock's (1987) classification scheme (Fig. 4b). The lamprophyres have variably high K_2O (3.4–6.9 wt%), with elevated K_2O/Na_2O ratios (1.4–4.0), exhibiting characteristic of potassic-ultrapotassic rocks, and plot within the ultrapotassic and shoshonitic field in the K_2O vs. Na_2O diagram (Fig. 4c; Foley et al., 1987). All samples plot between Groups I (lamproite) and III (orogenic lamprophyre-like) in the ultrapotassic discrimination diagram (Fig. 4d; Foley et al., 1987; Miller et al., 1999). The lamprophyres from the Lüchun-Jinping microblock have similar total alkalis contents and K_2O/Na_2O ratios as those of the western Churchill minettes (Fig. 4; Cousens et al., 2001).

The lamprophyres display coherent variation trends in Harker diagrams (Fig. 5). Contents of SiO_2 and Al_2O_3 negatively correlate with MgO, whereas FeO^T, TiO_2, Ba, Sr, and Ni positively correlate with MgO (Fig. 5). It is worth noting that when MgO is greater than 10%, there is an important turning point and a significant different trend for the CaO vs. Cr, as well as Ni/Cr and CaO/Al_2O_3 ratios (Fig. 5).

All lamprophyres from the different localities in the Lüchun-Jinping microblock show similar REE and trace element patterns (Fig. 6). They are characterized by LREE enrichment with a fractionated REE pattern, i.e. $(La/Sm)_N$ = 2.8–4.4 and $(Gd/Yb)_N$ = 2.1–4.3 (Table S3), without obvious Eu anomalies (Eu/Eu* = 0.73–0.91) (Fig. 6a). The ΣREE contents range from 136 to 254 ppm and the $(La/Yb)_N$ ratios vary from 9.6 to 25.4 (Table S3). The lamprophyres also show significant large-ion lithophile element (LILE) enrichment (e.g., Rb, Ba and K), and strong high-field strength element (HFSE) depletion (e.g., Zr, Hf and Nb). The significant negative Nb-Ta-Ti anomalies and the pronounced positive Pb spikes (Fig. 6b) observed in the lamprophyres are common features of arc-related volcanics (Hawkesworth et al., 1993).

4.3. Sr-Nd-Pb isotopes

The lamprophyres from the Lüchun-Jinping microblock have relatively high initial $^{87}Sr/^{86}Sr$ ratios of 0.7063–0.7078, but low initial $^{143}Nd/^{144}Nd$ ratios of 0.5124–0.5125, corresponding to εNd(t) values ranging from −3.9 to −2.4 (Table S3). They plot as an array in the enriched quadrant of the Sr—Nd isotope diagram (Fig. 7a). The Nd-isotope depleted mantle model ages (T_{DM}) range from 1484 to 1081 Ma (Table S3). Both $^{207}Pb/^{204}Pb$ (15.58–15.67) and $^{208}Pb/^{204}Pb$ (38.71–39.00) ratios are radiogenic, plotting as arrays well above the Northern Hemisphere Reference Line in the Pb isotope diagrams (Fig. 7c, d; NHRL, Hart, 1984). The Sr-Nd-Pb isotopic compositions of the lamprophyres in the Lüchun-Jinping microblock are within the range for the coeval potassic-ultrapotassic mafic rocks in western Yangtze Craton (Fig. 7; Guo et al., 2005; Huang et al., 2010; Lu et al., 2015).

5. Discussion

5.1. Timing of lamprophyres from the Lüchun-Jinping microblock

The relatively high Th/U (> 0.1) ratios and some of the well-

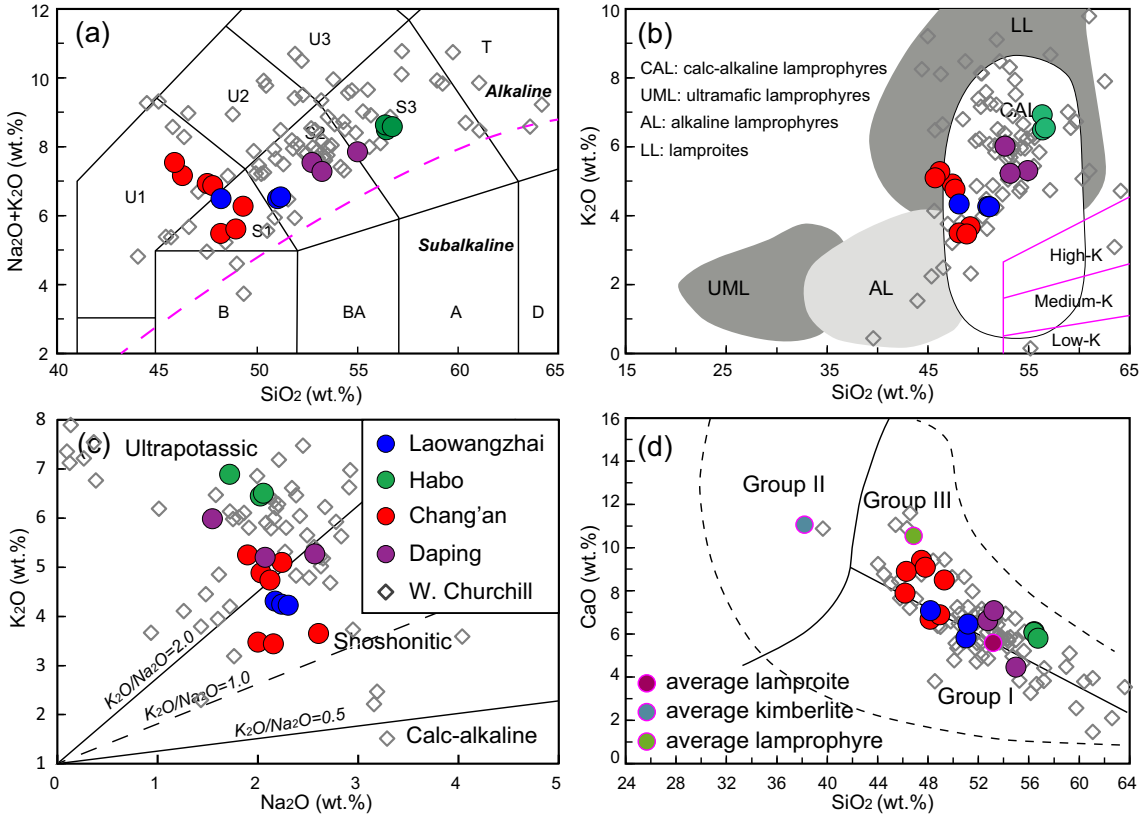

Fig. 4. Geochemical classification of lamprophyres from the Lüchun-Jinping microblock. (a) Total alkaline-silica diagram (Le Maitre, 2002). U1, tephrite; U2, phonotephrite; U3, tephriphonolite; S1, potassic trachybasalt; S2, shoshonite; S3, latite; T, trachyte; B, basalt; BA, basaltic andesite; A, andesite; and D, dacite. (b) K_2O vs. SiO_2 diagram (Rock, 1987). (c) K_2O vs. Na_2O diagram (Le Maitre, 2002). (d) Discrimination of ultrapotassic rocks into Groups I, II, and III based on the CaO vs. SiO_2 (Foley et al., 1987). Data of the minettes, from the western Churchill Province in NW Canada, are plotted for comparison (Cousens et al., 2001).

developed oscillatory or planar growth zoning in rim of zircons from the lamprophyres indicate a magmatic origin (Table S2; Fig. 3; Belousova et al., 2002). The zircons yield concordant U—Pb ages (Fig. 3), indicating that the $^{206}Pb/^{238}U$ weighted mean ages represent the timing of crystallization of lamprophyres from the Lüchun-Jinping microblock. Therefore, the lamprophyres from the Chang'an (CA14–116-1), Laowangzhai (LWZ1701–1) and Daping (DP17–1a) districts were emplaced at 34.7 ± 0.4 Ma, 34.6 ± 0.3 Ma, and 33.3 ± 0.3 Ma, respectively. These are consistent with the results of previous studies by different dating methods of the potassic-ultrapotassic mafic rocks in the Ailaoshan tectonic belt and western Yangtze Craton (Guo et al., 2005; Lu et al., 2015; Shen et al., 2021; Wang et al., 2001), as summarized in Table S1, and are similar to the adjacent intermediate-felsic intrusions along the Jinshajiang-Ailaoshan magma belt (37–32 Ma, Lu et al., 2012; Xu et al., 2012; Xin et al., 2020). Therefore, the lamprophyres from the Lüchun-Jinping microblock are the products of Eocene-Oligocene magmatism, possibly related to post-collisional transpressional and extensional tectonic settings at 42 to 26 Ma, following the India-Asia continental collision (Hou et al., 2007).

5.2. Examination of post-magmatic alteration

All lamprophyres collected for analysis are relatively fresh. A majority of the lamprophyres from the Lüchun-Jinping microblock have variable loss on ignition (LOI) contents (4.3–9.8 wt%, Table S3). These are similar to the variable LOI reflecting variable $H_2O + CO_2$ contents from the worldwide lamprophyre branches (Rock, 1987) and possibly due to different degrees of post-magmatic alteration (Zhou, 1999). The alteration effect on the major- and trace elements of the studied samples is assessed in Supplementary Fig. S2, grouped by their different localities.

The major elements (especially K_2O and Na_2O) and large-ion lithophile elements (LILEs) (e.g., Rb, Ba, Th) concentrations of all samples show no obvious correlation with LOI (Fig. S2), suggesting minimal modification of these elements due to post-magmatic alteration. The REEs, high-field strength elements (HFSEs) and compatible elements (e.g., Cr, Ni) are insoluble and thus remain immobile during intensive alteration (Hawkesworth et al., 1997). Additionally, $\varepsilon_{Nd}(t)$ and $(^{87}Sr/^{86}Sr)_i$ values do not correlate with LOI (Fig. S2), indicating that they were also unaffected by subsequent post-magmatic alteration. Therefore, the major and trace elements within lamprophyres behaved isochemically during post-magmatic processes.

5.3. Magmatic evolution

5.3.1. Fractional crystallization

The lamprophyres from the Lüchun-Jinping microblock have variable Mg# (100 × Mg/(Mg + Fe^{2+})) ranging from 66.0 to 78.6 (Table S3). The systematic variation between MgO and major and selected trace elements, and the subparallel REE patterns indicate fractional crystallization (Figs. 5, 6). The samples with MgO of 10 wt% approximate primitive melt compositions as they have Mg# of 70.0, which is assumed to be the Mg# value of melts in equilibrium with a peridotite source (Baker et al., 1995). The positive correlations between MgO and total FeO^T, and Cr and Ni, and the negative correlations between MgO and SiO_2, and Al_2O_3, indicate that olivine and clinopyroxene were fractionating phases (Fig. 5a, b, g, h, l). The samples with MgO < 10 wt% are characterized by negative correlation between MgO and Ni/Cr ratio, and positive correlations between MgO and CaO, and CaO/Al_2O_3 and Cr, indicating clinopyroxene-dominated fractionation (Fig. 5d, h, k, l). The negative correlation between MgO and Al_2O_3, and the positive correlations with Sr and Ba, and the minor negligible Eu

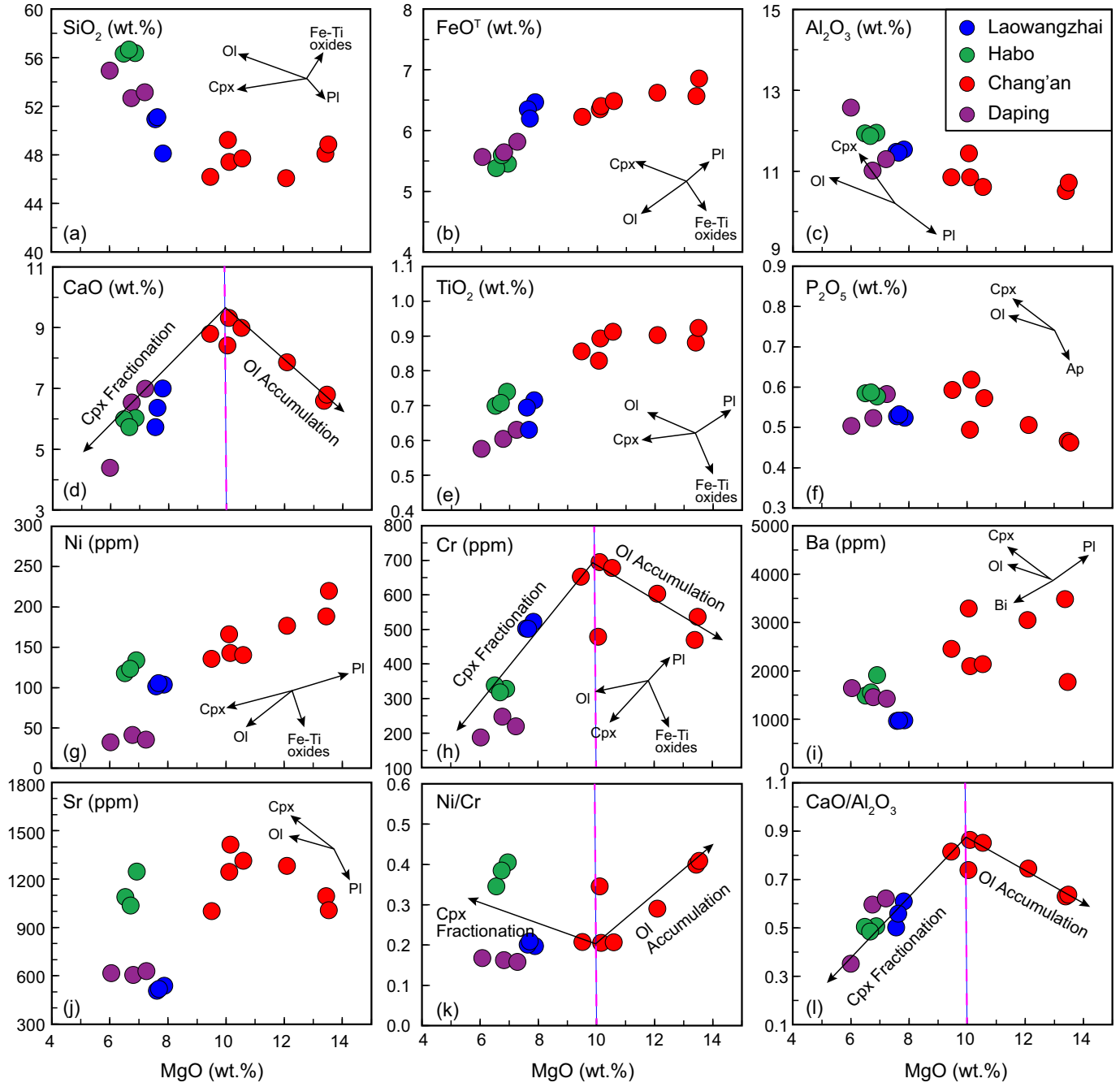

Fig. 5. MgO vs. selected major- and trace-elements for lamprophyres from the Lüchun-Jinping microblock, showing possible fractionating phases during magma evolution. The dotted vertical lines represent primitive melt with MgO = 10 wt%. The olivine (Ol) and clinopyroxene (Cpx) accumulation and fractionation vectors on CaO vs. MgO panel are after Huang et al. (2010).

anomalies, argue against significant plagioclase fractionation (Fig. 5c, 6). The lamprophyres with MgO > 10 wt% are most likely related to olivine accumulation as they have lower CaO and Cr contents and lower CaO/Al_2O_3 ratios, higher Ni contents, and higher Ni/Cr ratios than the primitive melt (Fig. 5d, g, h, k, l). These trends are similar to those of the contemporaneous basalts in western Yangtze Craton with olivine accumulation (Huang et al., 2010). The fractionating mineral assemblage of olivine + clinopyroxene can generally explain the variation trends in major and compatible trace elements of lamprophyres from the Lüchun-Jinping microblock.

5.3.2. *Crustal contamination*

The lamprophyres are mafic in terms of their low SiO_2 and high MgO contents, as well as enhanced concentrations of compatible elements (e.g., Cr and Ni) (Table S3). Collectively, the combination of high incompatible element contents (Rb, Ba, Th, U, K and LREEs), the depletion of Nb, Ta and Ti (Fig. 6), the low Ce/Pb (0.1–4.8) and Nb/U (1.7–4.0) ratios (Table S3), and the enriched Sr-Nd-Pb isotopic signatures (Fig. 7), suggests that an enriched component was involved in the genesis of lamprophyres from the Lüchun-Jinping microblock. Accordingly, it is critical to distinguish the crustal contamination process from mantle source enrichment.

Together with previous published data, the lamprophyres from the Lüchun-Jinping microblock have variable $\varepsilon_{Nd}(t)$ values (−0.4 to −11.4) (Fig. 7a; Table S3; Chen et al., 2014; Li et al., 2019; Yu et al., 2020) and abundant inherited zircon ages (Table S2; Fig. 3), which are possibly

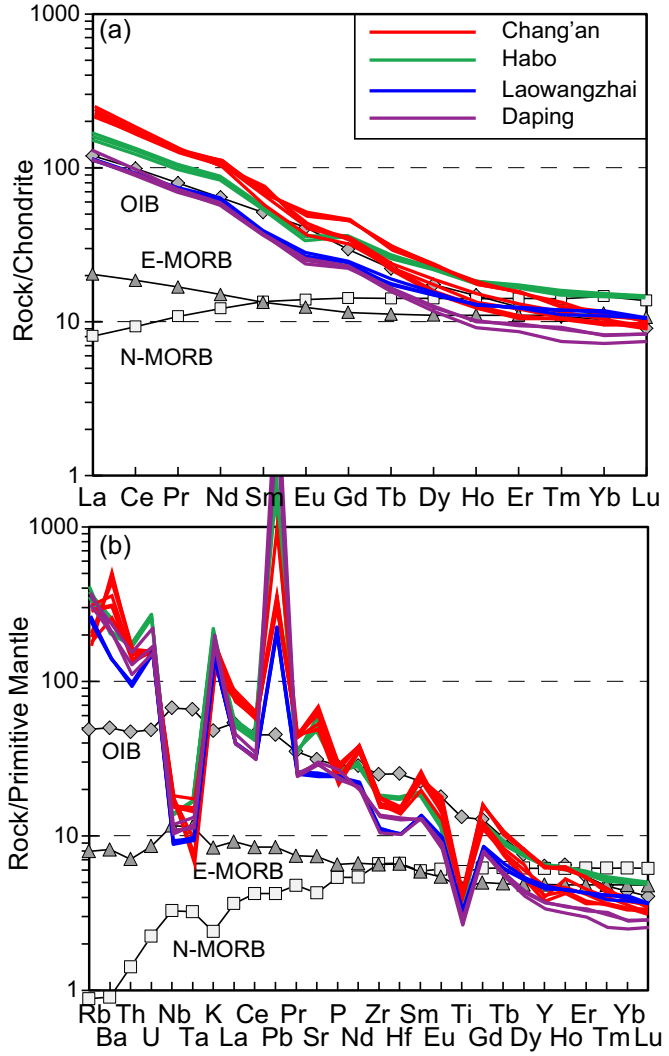

Fig. 6. (a) Chondrite-normalized rare earth element (REE) and (b) primitive mantle-normalized multi-element diagrams for lamprophyres from the Lüchun-Jinping microblock. Chondrite and primitive mantle normalizing values and the OIB, N-MORB and *E*-MORB values are from Sun and McDonough (1989).

consistent with variable degrees of crustal contamination. The $\varepsilon_{Nd}(t)$ values decrease with decreasing MgO for all but two cumulate samples, which also indicates crustal contamination during the emplacement of these lamprophyres (Fig. 7b; Li et al., 2002). However, the following lines of evidence suggest that these lamprophyres experienced only limited crustal contamination. Firstly, the Ba (977–3475 ppm) and Sr (509–1423 ppm) contents in the lamprophyres are much higher than those of average continental crust (390 ppm Ba, 325 ppm Sr; Rudnick and Fountain, 1995), suggesting the incompatible elements were not affected by crustal contamination. Second, mantle-derived magmas are characterized by low Lu/Yb ratios (0.14–0.15) whereas the continental crust has relatively higher Lu/Yb ratios (0.16–0.18) (Sun and McDonough, 1989). The lamprophyres have a somewhat variable, but generally low Lu/Yb ratios (0.13–0.15) (Table S3) indicating limited crustal contamination. Third and last, the lamprophyres have relatively uniform initial $^{87}Sr/^{86}Sr$ ratios (0.7063–0.7078) and Pb isotopic compositions (Fig. 7), and most lamprophyre samples have εNd(t) ranging between −0.4 and − 4.2, except for two samples with the lowest εNd(t) values (−8.0 and − 11.4) (Table S3; Chen et al., 2014; Li et al., 2019; Yu et al., 2020). Thus, in contrast to what was proposed by Chen et al. (2014), crustal contamination is limited and the geochemical signatures of lamprophyres from the Lüchun-Jinping microblock are probably related to an enriched mantle source that was variably enriched in LILEs and LREEs due to the earlier subduction-related metasomatism.

5.4. Petrogenesis of lamprophyres

5.4.1. Mineralogy and composition of the mantle source region

The lamprophyres from different localities in the Lüchun-Jinping microblock have similar whole-rock elemental and Sr-Nd-Pb isotopic compositions, indicating that they share an identical source. These lamprophyres are characterized by low SiO_2 (46.1–56.7 wt%) and high MgO (6.0–13.5 wt%) contents, high Mg# (66.1–78.6) and compatible elements (e.g., Cr = 187–692 ppm, Ni = 31–218 ppm) contents (Table S3), suggesting that they were derived from an ultramafic mantle source (Carmichael et al., 1996). Their enriched isotopic signatures exemplified by high initial $^{87}Sr/^{86}Sr$ ratios, negative $\varepsilon_{Nd}(t)$ values and high $^{206}Pb/^{204}Pb$ isotopic compositions, as well as the old T_{DM} ages (Fig. 7; Table S3), indicate that these lamprophyres originated from partial melting of enriched continental lithospheric mantle, rather than from a MORB- or an OIB-type asthenospheric mantle source. This conjecture is also supported by their trace element patterns (Fig. 6).

High K_2O (3.4–6.9 wt%) contents, elevated K_2O/Na_2O ratios (1.4–4.0), and significant LILEs enrichment of the lamprophyres from the Lüchun-Jinping microblock require potassium-rich mineral phases in the mantle source region. It has been suggested that volatile-bearing minerals such as phlogopite and amphibole are the major repositories for LILEs in the lithospheric mantle (Ionov et al., 1997). Since Rb and Ba are compatible in phlogopite, while Rb, Sr and Ba are moderately compatible in amphibole (LaTourrette et al., 1995), melts in equilibrium with phlogopite are expected to have significantly higher Rb/Sr (> 0.1) and lower Ba/Rb (⟨20) ratios (Furman and Graham, 1999). The lamprophyres have high Rb/Sr (0.10–0.39) and low Ba/Rb (5.43–32.9, mostly <20) ratios, indicating a predominance of phlogopite rather than amphibole in the melting source (Fig. 8a). The flat HREE normalized pattern and relatively high HREE abundances (e.g., Yb content is 10 times higher than in chondrite, Fig. 6a) in the lamprophyres are consistent with a spinel-facies mantle source rather than a garnet-facies mantle source, since HREEs are highly compatible in garnet (Turner et al., 1996). The geophysical inversions also indicate that the lithosphere thickness ranges from 80 to 100 km beneath the Lüchun-Jinping microblock (Hu et al., 2012), as a consequence of the convective lithospheric thinning after the Rayleigh-Taylor instability following the Indian-Asian collision. Moreover, experimental studies suggested that spinel is stable below 3.0 GPa (depth < 100 km) in pyrolite (Klemme and O'Neill, 2000). Low-degree (< 5%) partial melting of a hypothetical LREE-enriched spinel-facies mantle source ($[La/Yb]_N > 1$) can generate the La/Yb-Dy/Yb systematics of lamprophyres in the Lüchun-Jinping microblock (Fig. 8b).

5.4.2. Modification of the mantle source by subducted components

The lamprophyres collected from the Lüchun-Jinping microblock have high LILE concentrations, negative HFSEs (e.g., Nb, Ta and Ti) anomalies, and enriched Sr-Nd-Pb isotopic characteristics, which appear to be lacking in the convecting asthenosphere (Lu et al., 2015; Xu et al., 2001). As discussed above, having ruled out significant effects of crustal contamination, these compositional and isotopic features suggest that lamprophyres are indeed derived from an enriched lithospheric mantle, metasomatized by subducted slab components.

The depletion of HFSEs (i.e., Nb, Ta, and Ti) is recognized as a fingerprint of the subduction process (Hawkesworth et al., 1997). The Nb/U ratio is unaffected during variable degrees of partial melting and subsequent fractional crystallization, i.e. the Nb/U ratio of magmas can be used as a tracer for the source regions (Owen, 2008). The lamprophyres from the Lüchun-Jinping microblock have Nb/U ratios (1.69–3.99), which are significantly lower than those of the MORB/OIB (Nb/U = 47 ± 7), and the primitive and continental lithospheric mantle (Fig. 8c; Hofmann et al., 1986). Ayers (1998) suggested that subduction-

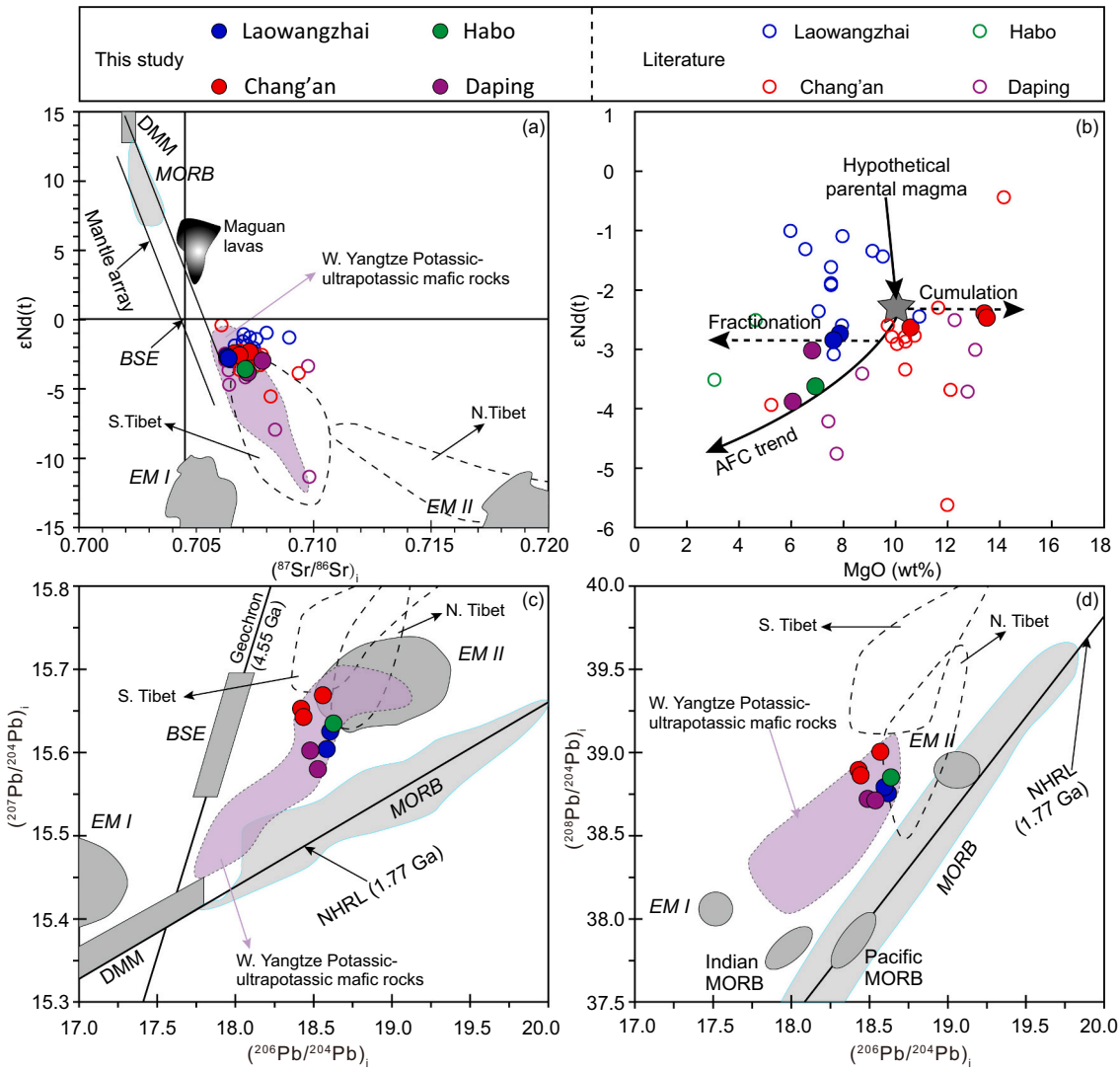

Fig. 7. Variation of (a) $(^{87}Sr/^{86}Sr)_i$ vs. $\varepsilon_{Nd}(t)$, (b) MgO vs. $\varepsilon_{Nd}(t)$, (c) $^{206}Pb/^{204}Pb$ vs. $^{207}Pb/^{204}Pb$, (d) $^{206}Pb/^{204}Pb$ vs. $^{208}Pb/^{204}Pb$ (after Li et al., 2002; Lu et al., 2015), for lamprophyres from the Lüchun-Jinping microblock. The field for western Yangtze mafic rocks is from Xu et al. (2001), Li et al. (2002), Guo et al. (2005), Huang et al. (2010) and Lu et al. (2015), the field for Cenozoic Maguan basalts is from Wang et al. (2001). The Northern Hemisphere Reference Line is from Hart (1984). Mantle reservoirs, BSE, MORB, DMM, EMI and EMII are from Zindler and Hart (1986). Indian MORB and Pacific MORB are after Guo et al. (2005). Data sources: Lamprophyres in the Chang'an, Habo, Laowangzhai and Daping districts from Zhu et al. (2013), Chen et al. (2014), Li et al. (2019) and Yu et al. (2020).

zone hydrous fluids have significantly low Nb/U ratio (< 0.22), which is ascribed to the transfer of significant amounts of LILEs in the slab-derived fluids. Accordingly, the lamprophyres are related to mantle sources with low Nb/U ratios beneath the Lüchun-Jinping microblock, which were metasomatized by subducted slab-derived hydrous fluids, rather than by the asthenospheric infiltration as suggested by Chen et al. (2014). However, oceanic slab subduction beneath the Lüchun-Jinping microblock did not occur when the lamprophyres formed at ca. 34 Ma (Deng et al., 2014; Metcalfe, 2013). Therefore, metasomatism is attributed to earlier subduction events during the Neoproterozoic and/or during the Late Permian-Triassic, along the edge of the Yangtze Craton (Guo et al., 2005; Lu et al., 2015; Zhou et al., 2006).

5.5. *The nature and evolution of lithospheric mantle beneath the Lüchun-Jinping microblock*

Various models have been proposed to explain the origin of metasomatiszed lithospheric mantle beneath southeastern Tibet. One model proposed that metasomatism occurred before 250 Ma, assuming that the Late Permian Emeishan mantle plume event at the edge of the Yangtze Craton would have purged the lithospheric mantle of all its fusible constituents (Huang et al., 2010; Xu et al., 2001). Following this assumption, the enriched lithospheric mantle beneath the southeastern Tibet has been interpreted to be exotic Tibetan lithosphere that extruded eastward under the craton during the Indian-Asian collision (Xu et al., 2001), or the metasomatism was the result of migrating melts originating from the seismic low velocity zone after 250 Ma (Huang et al., 2010). It has also been proposed that Proterozoic and possible Paleo-Tethyan Lancangjiang oceanic subduction caused metasomatism (Guo et al., 2005). An alternative explanation is that metasomatism was caused by Proterozoic oceanic subduction (Lu et al., 2015; Zhao and Zhou, 2007).

However, the lamprophyres in southeastern Tibet have different Sr-Nd-Pb isotope signatures compared to the potassic-ultrapotassic mafic rocks in northern and southern Tibet (Fig. 7; Lu et al., 2015). The lamprophyres from the Lüchun-Jinping microblock have higher εNd(t) and lower initial $^{87}Sr/^{86}Sr$ values than the potassic mafic rocks in Qiangtang terrane of northern Tibet, albeit with some overlap (Fig. 7a). Their Sr—Nd isotope signatures, however, are distinct from their mafic counterparts in Lhasa terrane of southern Tibet (Fig. 7a; Turner et al.,

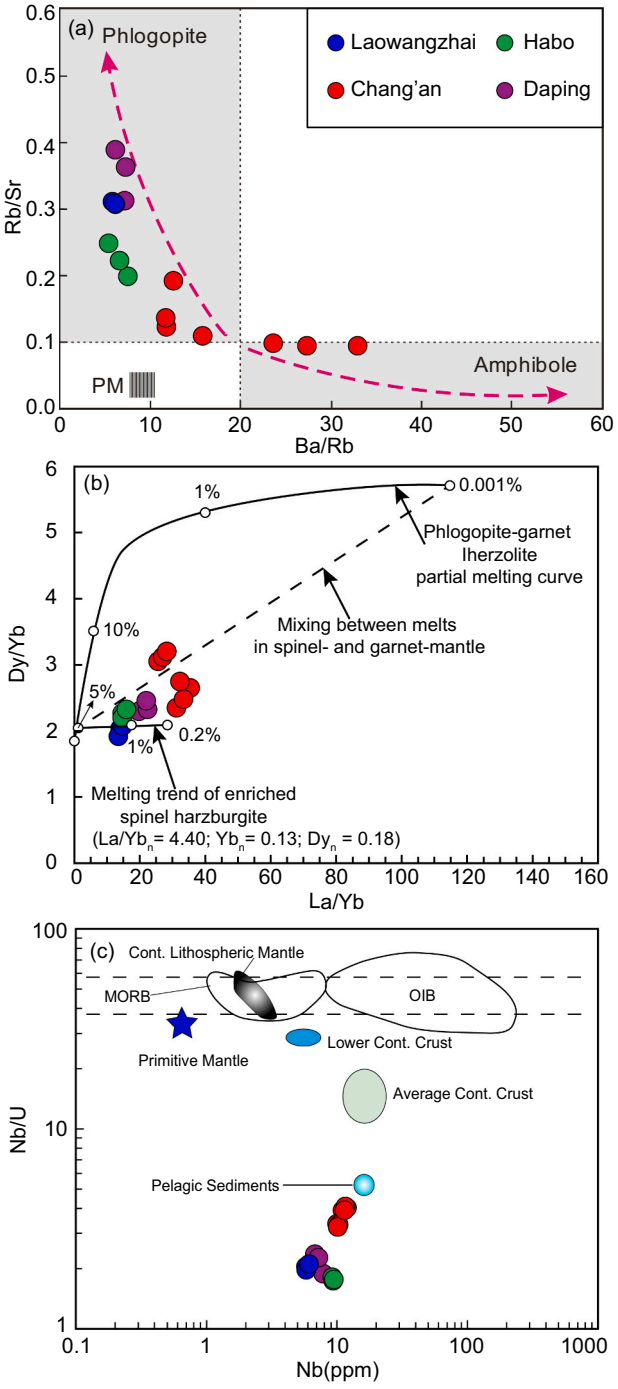

Fig. 8. (a) Rb/Sr vs. Ba/Rb diagram (Furman and Graham, 1999). (b) Dy/Yb vs. La/Yb diagram (Xu et al., 2001). Melting model, mode, and partition coefficients are following Xu et al. (2001). Source is phlogopite-bearing harzburgite with $(La/Yb)_N = 4.4$, $Yb_N = 0.13$ and $Dy_N = 0.18$. Source mineralogy is 70% olivine, 23% orthopyroxene, 5% clinopyroxene, and 2% spinel. (c) Nb vs. Nb/U (Owen, 2008) for lamprophyres from the Lüchun-Jinping microblock. OIB = oceanic-island basalt, MORB = mid-oceanic ridge basalt, PM = primitive mantle. Primitive mantle values are from Sun and McDonough (1989).

1996; Miller et al., 1999; Zhao et al., 2009). The Pb isotopic compositions of the lamprophyres in the Lüchun-Jinping microblock partly overlap with those of the potassic mafic rocks in Qiangtang terrane, but have distinct lower $^{207}Pb/^{204}Pb$ and $^{208}Pb/^{204}Pb$ values than the potassic mafic rocks in the Lhasa terrane (Fig. 7c, d; Turner et al., 1996; Miller et al., 1999). This is inconsistent with the hypothesis that the SCLM represents an exotic Tibetan lithosphere that was emplaced eastward beneath the Lüchun-Jinping microblock in southeastern Tibet during the Cenozoic.

The lamprophyres from the Lüchun-Jinping microblock are characterized by LILE enrichment (e.g., Ba, Rb, and Sr), HFSE depletion with significant Nb-Ta-Ti negative anomalies, and pronounced positive Pb anomlies (Fig. 6b). These geochemical characteristics do not support the hypothesis that metasomatism of the SCLM beneath the Lüchun-Jinping microblock was caused by a small-volume melt derived from the seismic low velocity zone. If that was the case, the lamprophyres in the Lüchun-Jinping microblock would have been characterized by HFSE enrichment and no distinct positive Pb spike (Hofmann, 2003).

Alternatively, metasomatism of lithosphere mantle beneath the Lüchun-Jinping microblock in southeastern Tibet could be attributed to a one-stage enrichment process associated with Proterozoic eastward oceanic subduction (Zhao and Zhou, 2007; Zhou et al., 2006). Subsequently, the metasomatically enriched SCLM was thermally eroded during the 260–250 Ma plume event, but residual metasomatic domains were partly preserved (Fig. 9; Lu et al., 2015), analogue to the western Churchill minettes, which have been reported in Canada (Cousens et al., 2001). In the Eocene-Oligocene post-collisional stage, the residual metasomatic domains were tapped, as the overthickened SCLM was removed, generating lamprophyres and mafic lavas in southeastern Tibet. This interpretation is supported by several lines of evidence outlined below.

The Panxi-Hannan arc volcanics and plutons in the west and north of the Yangtze Craton suggest Proterozoic (1000–740 Ma) eastward oceanic subduction beneath the edge of the Yangtze Craton, which extensively metasomatized the lithospheric mantle (Sun et al., 2009; Zhao and Zhou, 2007; Zhou et al., 2006). In addition, the amphibolites with Neoproterozoic ages in the Ailaoshan belt show arc-like geochemical features, including LILE enrichment and HFSE depletion, pronounced Nb, Ta and Ti depletion, and whole-rock εNd(t) values from −3.5 to −2.0 (Cai et al., 2014), indicating that the Ailaoshan tectonic belt was part of the Panxi-Hannan arc surrounding the western to northern margin of the Yangtze Craton.

The calculated Nd-depleted modal ages (T_{DM} = 1484–1081 Ma) of the sampled lamprophyres could be interpreted as the timing of the metasomatism event in the SCLM (Table S3; Turner et al., 1996). The western margin of the Yangtze Craton was a passive continental margin during the Late Neoproterozoic-Late Triassic (700–220 Ma), according to the westward subduction of Paleo-Tethys Jinshajiang-Ailaoshan oceanic slab, and characterized by deposition of carbonate and shale (Pullen et al., 2008). This further indicates that eastward subduction of the Paleo-Tethys Ailaoshan ocean was absent, and had not metasomatized the lithospheric mantle beneath the Lüchun-Jinping microblock during the closure of Paleo-Tethys Ailaoshan ocean.

In addition, the Eocene-Oligocene lamprophyres in the Lüchun-Jinping microblock and in western Yangtze Craton exhibit the same initial $^{143}Nd/^{144}Nd$-$^{87}Sr/^{86}Sr$ trend (Fig. 9a) as the SCLM-derived Neoproterozoic arc-related mafic rocks along the Ailaoshan tectonic belt and the western Yangtze Craton and the Late Permian Emeishan basalts in the Lüchun-Jinping microblock. This trend is different from the Early-Middle Permian Yaxuanqiao-Wusu arc basalts (Fig. 9a), indicating that these mafic rocks were derived from the same SCLM source (Fig. 9a; Zhou et al., 2006; Wang et al., 2007; Lu et al., 2015). Assuming that the $^{147}Sm/^{144}Nd$ ratios of Eocene-Oligocene lamprophyres reflect those of the mantle source, back calculation shows that the Neoproterozoic mafic arc rocks and Late Permian Emeishan basalts are well within the evolution trends defined by the lamprophyres (Fig. 9b), but the Early-Middle Permian Yaxuanqiao-Wusu arc basalts are out of the array (Fig. 9b). In summary, the Sr—Nd isotopic data support the hypothesis that metasomatism beneath the Lüchun-Jinping microblock in southeastern Tibet was only related to the Neoproterozoic (1000–740 Ma) eastward oceanic subduction and not related to the Paleo-Tethys Ailaoshan oceanic subduction.

It can be concluded that the lithospheric mantle source beneath the

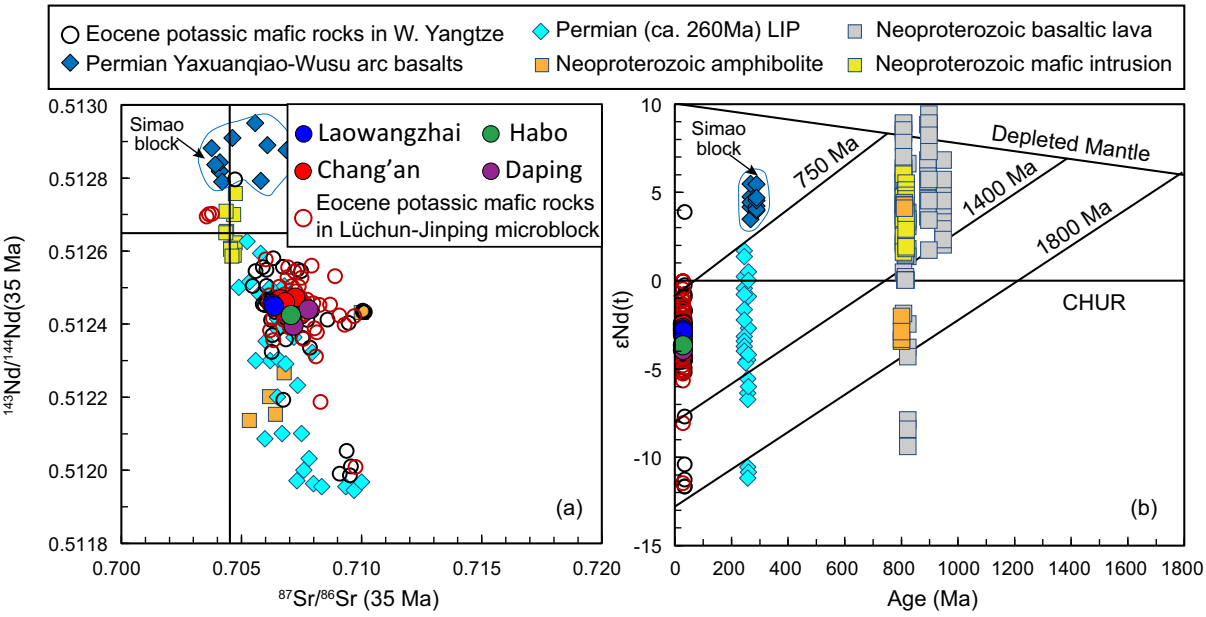

Fig. 9. Plots of (a) $^{143}Nd/^{144}Nd$ vs. $^{87}Sr/^{86}Sr$ and (b) εNd(t) vs. age for subcontinental lithospheric mantle (SCLM)-derived lamprophyres from the Lüchun-Jinping microblock (after Lu et al., 2015). (a) Eocene-Oligocene potassic-ultrapotassic mafic rocks from the Lüchun-Jinping microblock and western Yangtze Craton, showing that they have nearly the same Sr—Nd isotope values as the Emeishan SCLM-derived basalt and Neoproterozoic mafic intrusions. This indicates that they were derived from the same SCLM source. (b) Emeishan basalt and Neoproterozoic mafic rocks, showing that they are well within the evolution trends defined by Eocene-Oligocene potassic-ultrapotassic mafic rocks, also suggesting that they were derived from the same SCLM source. The 750, 1400 and 1800 Ma evolution curves in (b) are constructed using $^{147}Sm/^{144}Nd$ ratios of Eocene-Oligocene potassic-ultrapotassic mafic rocks assuming that the ratios reflect mantle sources. All Sr—Nd isotopic data have been recalculated at 35 Ma for comparison. Data sources: Neoproterozoic mafic intrusions (Li et al., 2006; Zhou et al., 2006); 260 Ma Emeishan basalt (Wang et al., 2007; Xiao et al., 2003); Early-Middle Permian Yaxuanqiao-Wusu arc basalts (Fan et al., 2010); Eocene-Oligocene potassic-ultrapotassic mafic rocks from the western Yangtze (Guo et al., 2005; Huang et al., 2010; Li et al., 2002; Lu et al., 2015; Xu et al., 2001), and from the Lüchun-Jinping microblock (Wang et al., 2001; Zhu et al., 2013; Chen et al., 2014; Li et al., 2019; Yu et al., 2020; Table S3).

Lüchun-Jinping microblock had undergone a similar geological evolutionary history as the enriched lithospheric mantle beneath the western Yangtze Craton (Fig. 9). Our geochemical investigations comply with the view that the Lüchun-Jinping microblock belongs to the Yangtze Craton rather than to the Simao-Indochina block, as already proposed by Chung et al. (1997). In addition, the location of the Late Permian collisional suture between the Simao-Indochina block and the Yangtze Craton is located >50 km west farther to the Ailaoshan shear zone (Fig. 1c; Chung et al., 1997). This conclusion that the Lüchun-Jinping microblock is a dismembered part of the Yangtze Craton, is supported by the following lines of evidence: (1) the lamprophyres from the Lüchun-Jinping microblock show numerous similarities with the potassic-ultrapotassic mafic rocks in western Yangtze Craton, including mineral assemblages, geochronology, and geochemical characteristics (Figs. 3, 7; Table S3; Guo et al., 2005; Lu et al., 2015); (2) there are abundant inherited zircons in lamprophyres from the Lüchun-Jinping microblock with Neoproterozoic ages (987–744 Ma, n = 29, Table S2). This is consistent with the peak crustal growth period (100–740 Ma) in western Yangtze Craton, which is associated with the Neoproterozoic underplating of arc basalts (Sun et al., 2009; Zhao and Zhou, 2007; Zhou et al., 2006); (3) the lamprophyres from the Lüchun-Jinping microblock show similar Sr-Nd-Pb isotopic compositions as the potassic-ultrapotassic mafic rocks in western Yangtze Craton (Fig. 7, 9a) The back calculation shows that the Neoproterozoic mafic rocks and Late Permian Emeishan basalts are well within the evolution trends defined by the lamprophyres, but different from the Early-Middle Permian Yaxuanqiao-Wusu arc basalts associated with the subduction of the Paleo-Tethys Ailaoshan ocean (Fig. 9).

5.6. *The compositional zonation constraints the paleo-position of the Lüchun-Jinping microblock*

The systematic variation of major and trace element contents with increasing distance to the Jinshajiang suture, identified in potassic-ultrapotassic mafic rocks from the western Yangtze Craton (Guo et al., 2005), appear to have petrogenetic significance and provide new constraints on the paleoposition of the Lüchun-Jinping microblock.

Compositional zonation of subduction-related igneous rocks across an island arc has been observed at many localities (Hochstaedter et al., 2000; Ryan et al., 1995). The origin of compositional zonation is dominantly controlled by the geochemical composition of the source region and the petrogenetic process (e.g., the degree of partial melting and magma differentiation) (Hochstaedter et al., 2000; Ryan et al., 1995). For example, previous studies have shown that different degrees of source depletion are a controlling factor in the compositional zonation of arc volcanics (Hochstaedter et al., 2000). However, the potassic-ultrapatossic mafic rocks show relatively little variation in Sr—Nd isotopic systematics (except for the mafic dykes from the Yao'an district, which are considerably scattered, Fig. 10a) with distance to the western margin of the Yangtze craton. This indicates that the mafic rocks share the same enriched lithospheric mantle domains as their magma sources (Guo et al., 2005; Lu et al., 2015; Xu et al., 2001). There was also no systematic magma differentiation variation observed with increasing distance to the western margin of the Yangtze craton. The MgO contents of the potassic-ultrapatossic mafic rocks show little variation with distance from the western margin to the craton interior (Fig. 11b), and all potassic-ultrapatossic mafic rocks have relatively high MgO, Ni, and Cr contents (Table S4). Thus, variable magma differentiation and/or crustal contamination that could potential cause compositional zonation in potassic-ultrapatossic mafic rocks can be excluded.

However, the potassic-ultrapatossic mafic rocks from the western

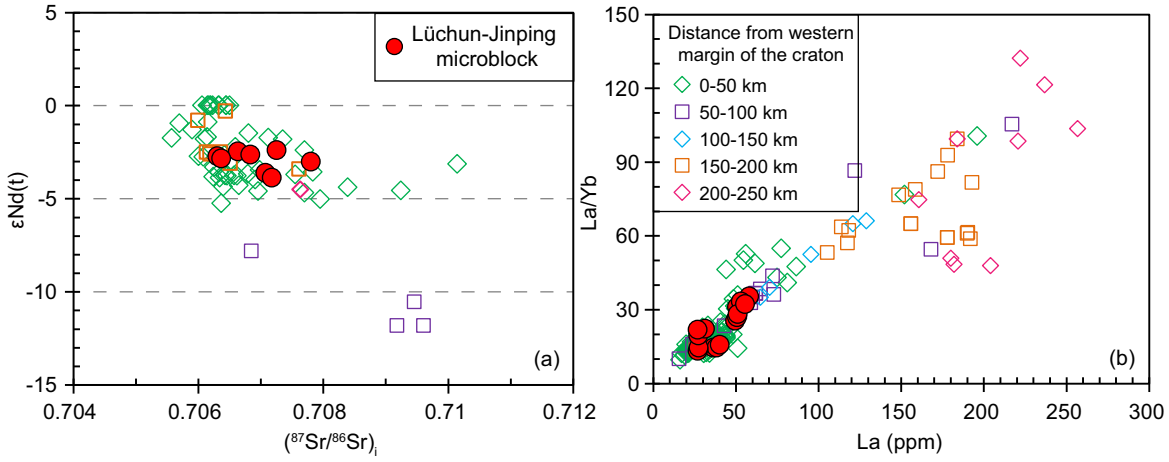

Fig. 10. (a) $(^{87}Sr/^{86}Sr)_i$ vs. $\varepsilon_{Nd}(t)$, (b) La vs. La/Yb for potassic-ultrapotassic mafic lavas and lamprophyres from the Lüchun-Jinping microblock and western Yangtze Craton. Data of Eocene-Oligocene potassic-ultrapotassic mafic rocks from the western Yangtze Craton are available in Table S4.

Yangtze Craton do demonstrate a positive correlation between La/Yb and La (Fig. 10b), suggesting that partial melting is a dominant process. Further, the La/Yb ratio shows an increasing trend with distance to the western margin of the craton (Fig. 11a), reflecting an increase in the degree of partial melting of the mantle source from the interior to the western margin.

In addition, the most striking characteristics of potassic-ultrapatossic mafic rocks from the western Yangtze Craton are the relatively high and variable LILE and LREE (e.g., Rb, Ba, Sr, Th, Ce and La; Fig. 11c, d, e) contents, indicating mantle source metasomatism by subduction-related fluids (Hawkesworth et al., 1997). The incompatible trace elements (e.g., Ba, Sr and Th) contents increase significantly with distance to the western margin of the Yangtze Craton (Fig. 11c, d, e). Incompatible element ratio variations (e.g., Ba/La, Sr/Ce and Ba/Rb) also show similar correlations (both positive and negative). This compositional zonation probably reflects changes in the amount of fluid added to the metasomatized mantle source region from which the potassic-ultrapatossic mafic rocks were derived (Guo et al., 2005). The systematic variation trends of incompatible element contents and ratios from the western margin to interior of the Yangtze Craton (Fig. 11) likely reflect a steady decline in the amount of subduction-derived metasomatic fluids introduced into the overlying mantle wedge (Hawkesworth et al., 1997).

In summary, the first-order controlling factors on the compositional zonation of potassic-ultrapatossic mafic rocks from the western Yangtze Craton should be the degree of partial melting and the amount of subduction-related fluid added to mantle source. The systemic geochemical trends (Fig. 11) imply that the lithospheric mantle beneath the more western margin parts of the Yangtze Craton underwent enrichment related to a relatively large amount of subduction-derived fluid that was introduced into the overlying lithospheric mantle and undergoing a high degree of partial melting. In contrast, the potassic-ultrapatossic mafic rocks situated in the interior part of the Yangtze Craton were derived from a lithospheric mantle source that was weakly modified by subduction-related fluids (i.e., with a relatively small amount of fluid added), and underwent a lower degree of partial melting.

Thus, the variation of compositional zonation of mafic magmas can be applied to (1) estimate the relative distance of melt segregation away from the margin of western Yangtze Craton, and (2) to reconstruct the precise paleogeography of the Lüchun-Jinping microblock based on comprehensive comparisons with the compositional zonation. Here, we combine the geochemical dataset of potassic-ultrapotassic mafic rocks from the western Yangtze Craton and the compositions of studied lamprophyres from the Lüchun-Jinping microblock to constrain the pre-Cenozoic paleogeographic location of the Lüchun-Jinping microblock. The lamprophyres from the Lüchun-Jinping microblock have relatively low LILE contents (e.g., Ba, Sr, and Th; Fig. 11c, d, e), and low La/Yb and Ba/Rb ratios (Fig. 11a, h). They show relatively elevated Ba/La and Sr/Ce ratios (Fig. 11f, g). These geochemical characteristics are comparable (or even more lower) to those of potassic-ultrapotassic mafic rocks from the western margin parts of the Yangtze Craton (e.g., Dali-Xiangyun, distance <50 km; Fig. 11), which indicates that the Lüchun-Jinping microblock was located in the most western part of Yangtze Craton and was closer to the Jinshajiang suture zone prior to the Cenozoic.

In addition, the comprehensive comparisons of the basaltic lava successions in the Jinping belt and the Binchuan Emeishan flood basalts show remarkably similar incompatible trace element patterns and consistent pre-Cretaceous chemo-stratigraphic variations (Chung et al., 1997; Xiao et al., 2003). This indicates that the basaltic lava successions in Jinping belt are a dismembered part of the Emeishan flood basalts, i.e. the paleoposition of the Lüchun-Jinping microblock was spatially at same paleolatitude as the Binchuan and in the western part of the Binchuan area during most of its geological history (Xiao et al., 2003). Furthermore, the paleomagnetic data of the lamprophyres and mineralized intrusions from the Beiya ore district in western Yangtze Craton and from the Chang'an gold district in the Lüchun-Jinping microblock also support this inference (Gao et al., 2018a, 2018b).

Considering the compositional zonation of the potassic-ultrapotassic mafic rocks in western Yangtze Craton (Figs. 10, 11), it can be concluded that the palaeogeographic position of the Lüchun-Jinping microblock was located near Dali area (west of the Binchuan area) before the Cenozoic, and even more closer to the Jinshajiang suture zone (Deng et al., 2014; Faure et al., 2014; Fig. 12). The current location of the Lüchun-Jinping microblock was resulted from the Oligocene sinistral movement and continental extrusion along the ASRR fault zone (Tapponnier et al., 1990; Chung et al., 1997; Liu et al., 2020; Fig. 12), which was a remote response to the India-Eurasia continental collision.

5.7. Geodynamic significance

The potassic mafic and felsic rocks in southeastern Tibet are coeval and were emplaced between 37 and 32 Ma along the Ailaoshan-Red River shear zone (Figs. 1, 3; Wang et al., 2001; Lu et al., 2012, 2015; Xu et al., 2012). Therefore, any tectonic model should explain the spatial and coeval nature of the potassic mafic and felsic rocks. The tectonic trigger for the generation of Eocene-Oligocene potassic rocks in southeastern Tibet remains controversial. It has been variously ascribed to sinistral movement along the Ailaoshan-Red River shear zone (Leloup et al., 1999), eastward continental subduction along strike-slip fault

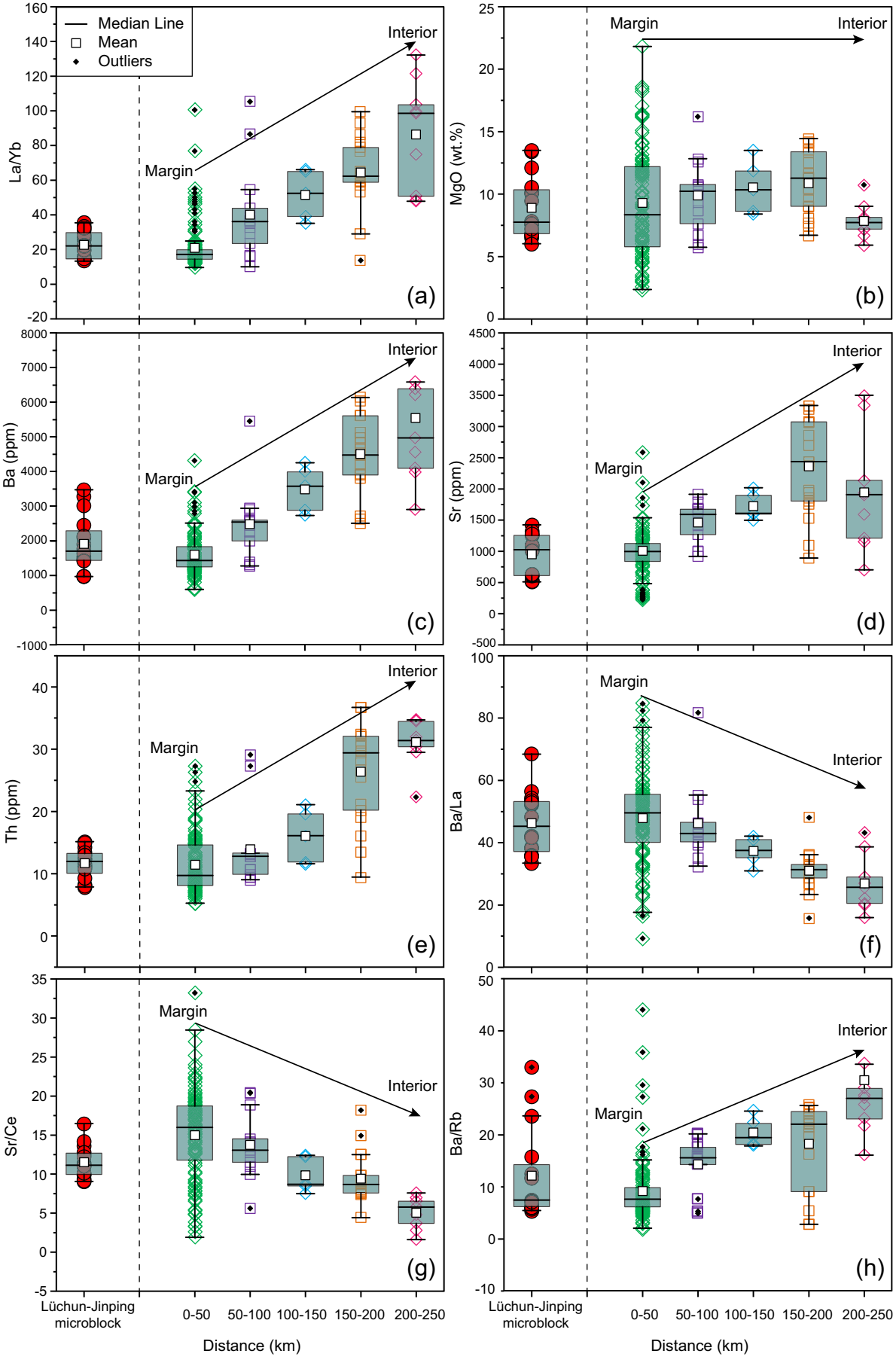

(caption on next page)

Fig. 11. Box and whisker plot of geochemical variation comparisons of lamprophyres from the Lüchun-Jinping microblock and potassic-ultrapotassic mafic rocks from the western Yangtze Craton (modified after Guo et al., 2005). Boxes show first to third quartile range with bars showing extremes of data (excluding any outliers). Legend as for Fig. 10. Line shows median value and square shows mean value. Arrow shows geochemical variation with increasing distance D (km) from the margin to interior of western Yangtze Craton. Data of potassic-ultrapotassic mafic rocks from the western Yangtze Craton refer to Table S4.

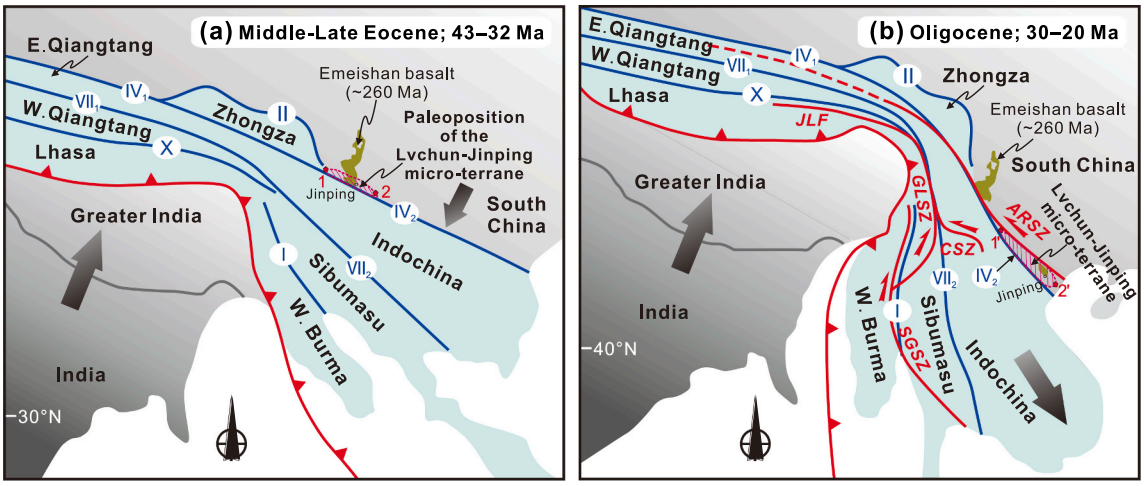

Fig. 12. Tectonic sketch map of southeastern Tibet showing the phased crustal deformation along the Jinshajiang Triassic suture and Ailaoshan-Red River shear zone, and the possible correlation of the Lüchun-Jinping microblock with the western margin of the Yangtze Craton (modified after Deng et al., 2014; Liu et al., 2020). Annotation: (I) Shan Boundary suture; (II) Garzê-Litang suture; (IV_1) Jinshajiang suture; (IV_2) Ailaoshan suture; (VII_1) Longmu Tso-Shuanghu suture; (VII_2) Changning-Menglian suture; (X) Banggong-Nujiang suture. Abbreviation: ARSZ, Ailaoshan-Red River shear zone; CSZ, Chongshan shear zone; GLGSZ, Gaoligongshan shear zone; JLF, Jiali fault; SGSZ, Saging shear zone. (a) Middle Eocene to Late Eocene (43–32 Ma), removal of lower lithospheric mantle caused the formation of potassic-ultrapotassic mafic rocks, and potassic felsic rocks along the Jinshajiang-Ailaoshan tectonic belt; (b) Oligocene (30–20 Ma), bending of southeastern Tibet resulting in the clockwise rotation of southern part from a NW strike to its present orientation, the extrusion of Indochina block, and the displacement along the Aillaoshan-Red River shear zone. The shearing-induced displacement offsets the potassic-ultrapotassic mafic rocks and potassic felsic rocks at the west side of the Aillaoshan-Red River shear zone. Positions 1 (Jianchuan) and 1′ (Laowangzhai) and 2 (Dali) and 2′ (Jinping) are equivalent, but displaced by the sinistral motion along the Ailaoshan-Red River shear zone. The Lüchun-Jinping microblock, between positions 1′ and 2′, is the missing segment between positions 1 and 2, and regarded as a dismembered part of western Yangtze Craton. The Late Permian basalts in the Lüchun-Jinping microblock are equivalent to the Binchuan Emeishan flood basalts (Xiao et al., 2003). (For interpretation of the references to colour in this figure legend, the reader is referred to the web version of this article.)

systems (Wang et al., 2001), and lithospheric thinning by convective removal of thickened lithospheric mantle (Chung et al., 1998; Lu et al., 2012).

However, sinistral ductile shearing occurred after 30 Ma based on the SHRIMP monazite Th—Pb data for three sets of leucocratic dykes within the shear zone yielding ages of 29.9 ± 0.5 Ma, 26.3 ± 0.5 Ma, 22.6 ± 0.3 Ma (Sassier et al., 2009). Furthermore, the *syn*- and post-kinematic leucogranite dykes yield zircon U—Pb ages of 28–23 Ma and 23–20 Ma, respectively, indicate that ductile shearing along the Ailaoshan-Red River shear zone occurred between 28 and 20 Ma (Liu et al., 2020). The new zircon U—Pb ages (34.7–33.3 Ma, Fig. 3), combined with published data (Wang et al., 2001; Xin et al., 2020; Zhu et al., 2013), imply that almost all potassic-ultrapotassic lamprophyres and potassic felsic intrusions in the Ailaoshan tectonic belt formed prior to ductile shearing, precluding a genetic relationship between sinistral shearing and potassic magmatism. In addition, the Eocene-Oligocene potassic magmas are not restricted to the Ailaoshan-Red River magmatic belt, but also occur between Yongping-Jianchuan proximal to the Ailaoshan-Red River shear zone, and Xichang in western Sichuan, which is ~270 km east of the shear zone (Guo et al., 2005; Lu et al., 2012), The Eocene-Oligocene potassic magmas were, therefore, widely developed in southeastern Tibet covering ~90,000 km^2 zone across the Simao Block and the Yangtze Craton (Fig. 1b). As a result, eastward continental subduction along strike-slip faults in southeastern Tibet can be ruled out as a controlling factor.

Thus, the Eocene-Oligocene potassic-ultrapotassic lamprophyres and basalts in southeastern Tibet were derived from extensively metasomatized lithospheric mantle, associated with the Neoproterozoic (1000–740 Ma) eastward oceanic subduction beneath the western Yangtze Craton (Fig. 13a; Zhou et al., 2006; Zhao and Zhou, 2007; Sun et al., 2009). The potassic felsic rocks with adakitic affinities may have been derived from partial melting of thickened mafic lower crust (Shen et al., 2021). The Cenozoic Indian-Asian collision caused progressive thickening of lithospheric mantle and crust beneath the western Yangtze Craton, southeastern Tibet (Fig. 13b; Chung et al., 2005). The crustal thickness beneath the western Yangtze Craton is currently 37–55 km, as indicated by seismic profiles (Wang et al., 2010). Melting of metasomatized SCLM and thickened lower crust generally requires an additional heat source as radiogenic heating is not sufficient to trigger melting due to the low thermal conductivity of mafic materials (Petford and Gallagher, 2001). One plausible mechanism for triggering melting of the SCLM and mafic lower crust is asthenosphere upwelling induced by the breakoff of Neo-Tethyan slab at 45–40 Ma (Fig. 1d; Lei and Zhao, 2016), in combination with the 42–32 Ma India-Eurasia continental hard collision causing diachronous removal of lower lithospheric mantle (Fig. 13c; Chung et al., 1998; Lu et al., 2012). Abundant Late Eocene-Oligocene rift basins in southeastern Tibet may be a subsequent consequence of extensional collapse after the lithospheric thinning (Chung et al., 1998; Wang et al., 2001). In addition, geophysical data imply that there is a ~ 300 km wide mantle diapir derived at ~450 km depth beneath the southeastern Tibet (Fig. 1d; Lei and Zhao, 2016). This also supports the hypothesis that the lower SCLM was convectively thined, and replaced by upwelling asthenospheric mantle material. Therefore, together with the absence of coeval mafic magma directly derived from asthenosphere in western Yangtze Craton (Chung et al., 1998; Xu et al., 2001), it is suggested that the upwelling asthenosphere and convective thinning of the lower SCLM was the geodynamic trigger for the generation of potassic-ultrapotassic mafic melts via melting of remnant metasomatized lithospheric mantle. The underplating of mantle-derived hot mafic magmas into thickened lower crust could induce partial melting of

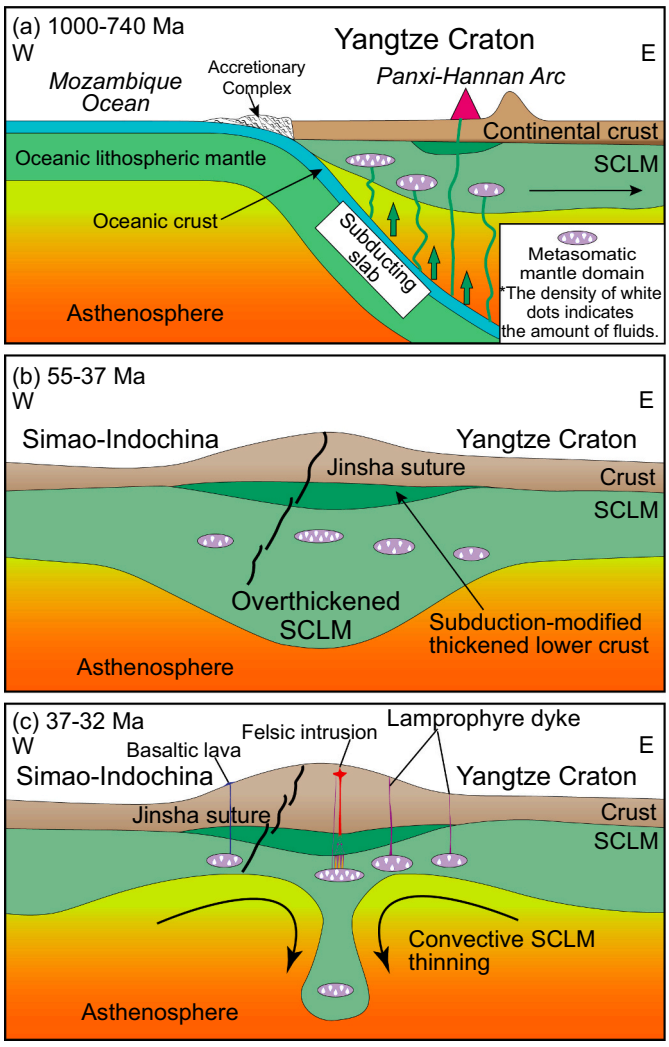

Fig. 13. Schematic diagrams (not to scale) illustrating the tectonic evolution and petrogenetic model for the formation of the post-collisional potassic-ultrapotassic mafic rocks in western Yangtze Craton. (a) In the Neoproterozoic, slab-derived fluids metasomatized the Yangtze continental lithospheric mantle (SCLM) producing many metasomatic domains. Subduction-related magmas underplated beneath the lower crust of Yangtze (modified from Zhou et al., 2006; Zhao and Zhou, 2007; Sun et al., 2009). The density of white dots in metasomatic mantle domain indicates the amount of subduction-related fluids added to mantle source. (b) Between 55 and 37 Ma, the continuing Indian-Asian collision preferentially overthickened the crust and SCLM along the Jinsha suture (modified from Lu et al., 2012). (c) In the Eocene (37–32 Ma), the lower part of overthickened lithospheric mantle adjacent to Jinsha suture was convectively removed, which led to upwelling of asthenosphere, partial melting of lower crust and metasomatic domains within residual SCLM (modified modified from Lu et al., 2015). Partial melting of residual SCLM produced potassic-ultrapotassic mafic magmas. Underplating of the mafic magmas beneath the bottom of the thickened lower crust resulted in melting of the mafic lower crust and the formation of adakitic magmas (after Shen et al., 2021).

thickened mafic lower crust resulting in the formation of felsic adakitic rocks (Lu et al., 2013; Shen et al., 2021; Fig. 13c).

6. Conclusions

The major conclusions of this contribution can be summarized as follows:

1. Zircon U—Pb geochronology shows that the emplacement ages of lamprophyres from the Lüchun-Jinping microblock occurred at 35–33 Ma. These lamprophyres were associated with post-collisional transpressional and extensional tectonic settings during the India-Asia continental collision.
2. The potassic-ultrapotassic lamprophyres in the Lüchun-Jinping microblock are characterized by LILE and LREE enrichment, HFSE depletion, high initial $^{87}Sr/^{86}Sr$ (0.7063–0.7078) values, negative $\varepsilon_{Nd}(t)$ values (−3.9 to −2.4), and old Nd model ages (1484–1081 Ma). These geochemical features, combined with low Nb/U ratios, indicate that the lamprophyres were derived from partial melting of enriched lithospheric mantle, metasomatized by subduction-related fluids beneath the Lüchun-Jinping microblock, and responsible for the convective thinning of overthickened lithospheric mantle following the India-Asia collision.
3. Separation of the lamprophyres in the Lüchun-Jinping microblock is identified as a dismembered part of western Yangtze Craton, and escaped along the Ailaoshan-Red River shear zone due to Cenozoic sinistral movement. Identification of these Eocene-Oligocene lamprophyres, which are comparable to potassic-ultrapotassic mafic rocks from the western Yangzte Craton, and comprehensive comparisons with the composition zonation indicate that the paleogeography of the Lüchun-Jinping microblock was near the Dali area (west of the Binchuan) and close to the Jinshajiang suture zone before the Cenozoic.

Supplementary data to this article can be found online at https://doi.org/10.1016/j.lithos.2022.106622.

Declaration of Competing Interest

The authors declare that they have no known competing financial interests or personal relationships that could have appeared to influence the work reported in this paper.

Acknowledgements

We would like to thank Prof. Xian-Hua Li for his editorial assistance. We are grateful to Prof. Michel Faure and two anonymous reviewers, for their thorough and constructive reviews, which greatly improved this manuscript. We also would like to thank Drs. Qiang Fu and Xiao-Yan Zhao for fieldwork assistances and valuable discussions. This work was financially supported by the National Key Research and Development Program of China (grant numbers 2019YFA0708602 and 2016YFC0600310), the National Natural Science Foundation of China (grant numbers 42022014 and 41872083), the Yunnan Fundamental Research Projects (grant number 202101AT070073), the China Fundamental Research Funds for the Central Universities (grant number 2652018133) and a fellowship from the China Scholarship Council (CSC number 201906400047). This is contribution PGC-201585 from the China University of Geosciences, Beijing (petro-geochemistry).

References

Ayers, J., 1998. Trace element modeling of aqueous fluid–peridotite interaction in the mantle wedge of subduction zones. Contrib. Mineral. Petrol. 132, 390–404.
Baker, M.B., Hischmann, M.M., Ghiorso, M.S., Stolper, E.M., 1995. Compositions of nearsolidus predictive melts from experiments and thermodynamic calculations. Nature 375, 308–311.
Belousova, E., Griffin, W., O'Reilly, S., Fisher, N., 2002. Igneous zircon: trace element composition as an indicator of source rock type. Contrib. Mineral. Petrol. 143, 602–622.
Cai, Y.F., Wang, Y.J., Cawood, P.A., Fan, W.M., Liu, H.C., Xing, X.W., Zhang, Y.Z., 2014. Neoproterozoic subduction along the Ailaoshan zone, South China: geochronological and geochemical evidence from amphibolite. Precambrian Res. 245, 13–28.
Carmichael, I.S.E., Lange, R.A., Luhr, J.F., 1996. Quaternary minettes and associated volcanic rocks of Mascota, western Mexico: a consequence of plate extension above a subduction modified mantle wedge. Contrib. Mineral. Petrol. 124, 302–333.
Chen, Y.H., Yao, S.Z., Pan, Y.M., 2014. Geochemistry of lamprophyres at the Daping gold deposit, Yunnan Province, China: Constraints on the timing of gold mineralization and evidence for mantle convection in the eastern Tibetan Plateau. J. Asian Earth Sci. 93, 129–145.

Chung, S.L., Lee, T.Y., Lo, C.H., Wang, P.L., Chen, C.Y., Yem, N.T., Hoa, T.T., Wu, G.Y., 1997. Intraplate extension prior to continental extrusion along the Ailao Shan–Red River shear zone. Geology 25, 311–314.
Chung, S.L., Lo, C.H., Lee, T.Y., Zhang, Y.Q., Xie, Y.W., Li, X.H., Wang, K.L., Wang, P.L., 1998. Diachronous uplift of the Tibetan plateau starting 40 Myr ago. Nature 394, 769–773.
Chung, S.L., Chu, M.F., Zhang, Y.Q., Xie, Y.W., Lo, C.H., Lee, T.Y., Lan, C.Y., Li, X.H., Zhang, Q., Wang, Y.Z., 2005. Tibetan tectonic evolution inferred from spatial and temporal variations in post-collisional magmatism. Earth-Sci. Rev. 68, 173–196.
Cocks, L., Torsvik, T.H., 2013. The dynamic evolution of the Palaeozoic geography of eastern Asia. Earth Sci. Rev. 117, 40–79.
Conticelli, S., Guarnieri, L., Farinelli, A., Mattei, M., Avanzinelli, R., Bianchini, G., Boari, E., Tommasini, S., Tiepolo, M., Prelevic, D., Venturelli, G., 2009. Trace elements and Sr–Nd–Pb isotopes of K-rich, shoshonitic, and calc-alkaline magmatism of the Western Mediterranean Region: genesis of ultrapotassic to calc-alkaline magmatic associations in a post-collisional geodynamic setting. Lithos 107, 68–92.
Cousens, B.L., Aspler, L.B., Chiarenzelli, J.R., Donaldson, J.A., Sandeman, H., Peterson, T.D., Lecheminant, A.N., 2001. Enriched Archean lithospheric mantle beneath western Churchill Province tapped during Paleoproterozoic orogenesis. Geology 29, 827–830.
Deng, J., Wang, Q.F., Li, G.J., Santosh, M., 2014. Cenozoic tectono-magmatic and metallogenic processes in the Sanjiang region, southwestern China. Earth-Sci. Rev. 138, 268–299.
Fan, W.M., Wang, Y.J., Zhang, A.M., Zhang, F.F., Zhang, Y.Z., 2010. Permian arc-back-arc basin development along the Ailaoshan tectonic zone: Geochemical, isotopic and geochronological evidence from the mojiang volcanic rocks, southwest china. Lithos 119, 553–568.
Faure, M., Lepvrier, C., Nguyen, V.V., Vu, T.V., Lin, W., Chen, Z.C., 2014. The South China block-Indochina collision: where, when, and how? J. Asian Earth Sci. 79, 260–274.
Faure, M., Lin, W., Yang, C., Lepvrier, C., 2016. Triassic tectonics of the Ailaoshan Belt (SW China): early Triassic collision between the South China and Indochina blocks, and Middle Triassic intracontinental shearing. Tectonophysics 683, 27–42.
Foley, S., 1992. Vein-plus-wall-rock melting mechanisms in the lithosphere and the origin of potassic alkaline magmas. Lithos 28, 435–453.
Foley, S.F., Venturelli, G., Green, D.H., Toscani, L., 1987. The ultrapotassic rocks: Characteristics, classification, and constraints for petrogenetic models. Earth-Sci. Rev. 24, 81–134.
Furman, T., Graham, D., 1999. Erosion of lithospheric mantle beneath the East African Rift system: geochemical evidence from the Kivu volcanic province. Developments in Geotectonics 24, 237–262.
Gao, L., Deng, J., Wang, Q.F., Zhang, S.H., Yang, Z.Y., 2018a. New Paleomagnetic results from the Beiya porphyry-skarn gold–polymetallic deposit at the Western Dali faulted-block: Implications for the Cenozoic tectonic rotation of the Chuan-Dian Fragment, Southeastern Tibetan Plateau. Tectonophysics 747–748, 163–176.
Gao, L., Wang, Q.F., Deng, J., Zhang, S.H., Yang, Z.Y., 2018b. Relationship between orogenic gold mineralization and crustal shearing along Ailaoshan–Red River Belt, southeastern Tibetan Plateau: new constraint from paleomagnetism. G-cubed 19, 2225–2242.
Guo, Z.F., Hertogen, J.A.N., Liu, J.Q., Pasteels, P., Boven, A., Punzalan, L.E.A., He, H.Y., Luo, X.J., Zhang, W.H., 2005. Potassic Magmatism in Western Sichuan and Yunnan Provinces, SE Tibet, China: Petrological and Geochemical Constraints on Petrogenesis. J. Petrol. 46, 33–78.
Hart, S.R., 1984. A large-scale isotope anomaly in the southern hemisphere mantle. Nature 309, 753–757.
Hawkesworth, C.J., Gallagher, K., Hergt, J.M., McDermott, F., 1993. Mantle and Slab Contributions in ARC Magmas. Annu. Rev. Earth Planet. Sci. 21, 175–204.
Hawkesworth, C.J., Turner, S.P., McDermott, F., Peate, D.W., van Calsteren, P., 1997. U–Th isotopes in arc magmas: implications for element transfer from the subducted crust. Science 276, 551–555.
Hennig, D., Lehmann, B., Frei, D., Belyatsky, B., Zhao, X.F., Cabral, A.R., Zeng, P.S., Zhou, M.F., Schmidt, K., 2009. Early permian seafloor to continental arc magmatism in the eastern Paleo-Tethys: U–Pb age and Nd-Sr isotope data from the southern Lancangjiang zone, Yunnan, China. Lithos 113, 408–422.
Hochstaedter, A.G., Gill, J.B., Taylor, B., Ishizuka, O., Yuasa, M., Morita, S., 2000. Across-arc geochemical trends in the Izu–Bonin arc: constraints on source composition and mantle melting. J. Geophys. Res. 105, 495–512.
Hofmann, A.W., 2003. Sampling mantle heterogeneity through oceanic basalts: Isotopes and trace elements. In: Rudnick, R.L. (Ed.), The Crust, Treatise on Geochemistry, vol. 2, pp. 61–101.
Hofmann, A.W., Jochum, K.P., Seufert, M., White, W.M., 1986. Nb and Pb in oceanic basalts: new constraints on mantle evolution. Earth Planet. Sci. Lett. 79, 33–45.
Hou, Z.Q., Zaw, K., Pan, G.T., Mo, X.X., Xu, Q., Hu, Y.Z., Li, X.Z., 2007. Sanjiang Tethyan metallogenesis in S.W. China: Tectonic setting, metallogenic epochs and deposit types. Ore Geol. Rev. 31, 48–87.
Hu, J.F., Yang, H.Y., Xu, X.Q., Wen, L.M., Li, G.Q., 2012. Lithospheric structure and crust–mantle decoupling in the southeast edge of the Tibetan Plateau. Gondwana Res. 22, 1060–1067.
Huang, X.L., Niu, Y.L., Xu, Y.G., Chen, L.L., Yang, Q.J., 2010. Mineralogical and geochemical constraints on the petrogenesis of post-collisional potassic and ultrapotassic rocks from western Yunnan, SW China. J. Petrol. 51, 1617–1654.
Ionov, D.A., Griffin, W.L., O'Reilly, S.Y., 1997. Volatile-bearing minerals and lithophile trace elements in the upper mantle. Chem. Geol. 141, 153–184.
Klemme, S., O'Neill, H.S.C., 2000. The near-solidus transition from garnet lherzolite to spinel lherzolite. Contrib. Mineral. Petrol. 138, 237–248.
LaTourrette, T., Hervig, R.L., Holloway, J.R., 1995. Trace element partitioning between amphibole, phlogopite, and basanite melt. Earth Planet. Sci. Lett. 135, 13–30.
Le Maitre, R.W., 2002. Igneous Rocks: A Classification and Glossary of Terms: Recommendations of the International Union of Geological Sciences Subcommission on the Systematics of Igneous Rocks. Cambridge University Press, Cambridge, p. 208.
Lei, J.S., Zhao, D.P., 2016. Teleseismic P-wave tomography and mantle dynamics beneath Eastern Tibet. Geochem., Geophys. Geosyst. 17, 1861–1884.
Leloup, P.H., Lacassin, R., Tapponnier, P., Schärer, U., Zhong, D.R., Liu, X.H., Zhang, L. Z., Ji, S.C., Trinh, P.T., 1995. The Ailao Shan–Red River shear zone (Yunnan, China), tertiary transform boundary of Indochina. Tectonophysics 251, 3–84.
Leloup, P.H., Ricard, Y., Battaglia, J., Lacassin, R., 1999. Shear heating in continental strike-slip shear zone: numerical modelling and case studies. Geophys. J. Int. 136, 19–40.
Li, X.H., Zhou, H.W., Chung, S.L., Lo, C.H., Wei, G.J., Liu, Y., Lee, C.Y., 2002. Geochemical and Sr–Nd isotopic characteristics of late paleogene ultrapotassic magmatism in Southeastern Tibet. Int. Geol. Rev. 44, 559–574.
Li, X.H., Li, Z.X., Sinclair, J.A., Li, W.X., Carter, G., 2006. Revisiting the "Yanbian Terrane": Implications for Neoproterozoic tectonic evolution of the western Yangtze Block, South China. Precambrian Res. 151, 14–30.
Li, H.J., Wang, Q.F., Groves, D.I., Deng, J., Dong, C.Y., Wang, X., Yang, L., 2019. Alteration of Eocene lamprophyres in the Zhenyuan orogenic gold deposit, Yunnan Province, China: Composition and evolution of ore fluids. Ore Geol. Rev. 107, 1068–1083.
Liu, J.L., Chen, X.Y., Tang, Y., Song, Z.J., Wang, W., 2020. The Ailao Shan−Red River shear zone revisited: timing and tectonic implications. GSA Bull. 132, 1165–1182.
Lu, Y.J., Kerrich, R., Cawood, P.A., McCuaig, T.C., Hart, C.J.R., Li, Z.X., Hou, Z.Q., Bagas, L., 2012. Zircon SHRIMP U–Pb geochronology of potassic felsic intrusions in western Yunnan, SW China: Constraints on the relationship of magmatism to the Jinsha suture. Gondwana Res. 22, 737–747.
Lu, Y.J., McCuaig, T.C., Li, Z.X., Jourdan, F., Hart, C.J.R., Hou, Z.Q., Tang, S.H., 2015. Paleogene post-collisional lamprophyres in western Yunnan, western Yangtze Craton: Mantle source and tectonic implications. Lithos 233, 139–161.
Metcalfe, I., 2013. Gondwana dispersion and Asian accretion: Tectonic and palaeogeographic evolution of eastern Tethys. J. Asian Earth Sci. 66, 1–33.
Miller, C., Schuster, R., Klotzli, U., Frank, W., Purtscheller, F., 1999. Post-collisional potassic and ultrapotassic magmatism in SW Tibet: geochemical and Sr–Nd–Pb–O isotopic constraints for mantle source characteristics and petrogenesis. J. Petrol. 40, 1399–1424.
Müller, D., Groves, D.I., 2000. Indirect associations between lamprophyres and gold–copper deposits. In: Potassic Igneous Rocks and Associated Gold–Copper Mineralization, Vol. 7. Springer, Berlin, Heidelberg, p. 143.
Owen, J.P., 2008. Geochemistry of lamprophyres from the Western Alps, Italy: implications for the origin of an enriched isotopic component in the Italian mantle. Contrib. Mineral. Petrol. 155, 341–362.
Pan, G., Xu, Q., Hou, Z., Wang, L., Du, D., Mo, X., Li, D., Wang, M., Li, X., Jiang, X., Hu, Y., 2003. Archipelagic Orogenesis, Metallogenic Systems and Assessment of the Mineral Resources along the Nüjiang-Lancangjiang-Jinshajiang Area in Southwestern China. Geological Publishing House, Beijing (in Chinese with English abstract).
Petford, N., Gallagher, K., 2001. Partial melting of mafic (amphibolitic) lower crust by periodic in flux of basaltic magma. Earth Planet. Sci. Lett. 193, 483–499.
Prelević, D., Akal, C., Foley, S.F., Romer, R.L., Stracke, A., Bogaard, P.V.D., 2012. Ultrapotassic mafic rocks as geochemical proxies for post-collisional dynamics of orogenic lithospheric mantle: the case of Southwestern Anatolia, Turkey. J. Petrol. 53, 1019–1055.
Pullen, A., Kapp, P., Gehrels, G.E., Vervoort, J.D., Ding, L., 2008. Triassic continental subduction in central Tibet and Mediterranean-style closure of the Paleo-Tethys Ocean. Geology 36, 351–354.
Rock, N.M.S., 1987. The nature and origin of lamprophyres: an overview. In: Fitton, J.G., Upton, B.G. (Eds.), Geol. Soc., London, Spec. Publ, 30, pp. 191–226. The Alkaline Igneous Rocks.
Rudnick, R.L., Fountain, D.M., 1995. Nature and composition of the continental crust: a lower crustal perspective. Rev. Geophys. 33, 267–309.
Ryan, J.G., Morris, J., Tera, F., Leeman, W.P., Tsvetskov, A., 1995. Cross-arc geochemical variations in the Kurile arc as a function of slab depth. Science 270, 625–627.
Sassier, C., Leloup, P.H., Rubatto, D., Galland, O., Yue, Y., Ding, L., 2009. Direct measurement of strain rates in ductile shear zones: a new method based on syntectonic dikes. J. Geophys. Res.: Solid Earth 114, B01406. https://doi.org/10.1029/2008JB00597.
Shen, Y., Zheng, Y.C., Hou, Z.Q., Zhang, A.P., Huizenga, J.M., Wang, Z.X., Wang, L., 2021. Petrology of the Machangqing complex in Southeastern Tibet: implications for the genesis of potassium-rich adakite-like intrusions in collisional zones. J. Petrol. https://doi.org/10.1093/petro logy/egab066.
Sone, M., Metcalfe, I., 2008. Parallel Tethyan sutures in mainland Southeast Asia: new insights for Palaeo-Tethys closure and implications for the Indosinian orogeny. Compt. Rendus Geosci. 340, 166–179.
Sun, S.S., McDonough, W.F., 1989. Chemical and isotopic systematics of oceanic basalts: Implications for mantle composition and processes. In: Saunders, A.D., Norry, M.J. (Eds.), Magmatism in the Ocean Basins, Geol. Soc., London, Spec. Publ, 42, pp. 313–345.
Sun, W.H., Zhou, M.F., Gao, J.F., Yang, Y.H., Zhao, X.F., Zhao, J.H., 2009. Detrital zircon U-Pb geochronological and Lu-Hf isotopic constraints on the Precambrian magmatic and crustal evolution of the western Yangtze Block, SW China. Precambrian Res. 172, 99–126.

Tapponnier, P., Lacassin, R., Leloup, P.H., Schaer, U., Zhong, D.L., Liu, X.H., Ji, S.C., Zhang, L.S., Zhong, J.Y., 1990. The Ailao Shan/Red River metamorphic belt: Tertiary left-lateral shear between Indochina and South China. Nature 343, 431–437.

Turner, S., Arnaud, N., Liu, J., Rogers, N., Hawkesworth, C., Harris, N., Kelley, S., Van Calsteren, P., Deng, W., 1996. Post-collision, Shoshonitic Volcanism on the Tibetan Plateau: implications for convective thinning of the lithosphere and the source of ocean island basalts. J. Petrol. 37, 45–71.

Wang, J.H., Yin, A., Harrison, T.M., Grove, M., Zhang, Y.Q., Xie, G.H., 2001. A tectonic model for Cenozoic igneous activities in the eastern Indo–Asian collision zone. Earth Planet. Sci. Lett. 188, 123–133.

Wang, C.Y., Zhou, M.F., Qi, L., 2007. Permian flood basalts and mafic intrusions in the Jinping (SW China) –Song Da (northern Vietnam) district: Mantle sources, crustal contamination and sulfide segregation. Chem. Geol. 243, 317–343.

Wang, P., Wang, L.S., Mi, N., Liu, J.H., Li, H., Yu, D.Y., Xu, M.J., Wang, X.C., Guo, Z.W., 2010. Crustal thickness and average Vp/Vs ratio variations in southwest Yunnan, China, from teleseismic receiver functions. J. Geophys. Res. 115 (B11308), 2010. https://doi.org/10.1029/2009JB006651.

Wang, Q.F., Deng, J., Li, C., Li, G.J., Yu, L., Qiao, L., 2014. The boundary between the Simao and Yangtze blocks and their locations in Gondwana and Rodinia: constraints from detrital and inherited zircons. Gondwana Res. 26, 438–448.

Wang, Y.J., Zhou, Y.Z., Cai, Y.F., Liu, H.C., Zhang, Y.Z., Fan, W.M., 2016. Geochronological and geochemical constraints on the petrogenesis of the Ailaoshan granitic and migmatite rocks and its implications on Neoproterozoic subduction along the SW Yangtze Block. Precambrian Res. 283, 106–124.

Xiao, L., Xu, Y.G., Chung, S.L., He, B., Mei, H.J., 2003. Chemostratigraphic correlation of upper permian lavas from yunnan province, china: extent of the emeishan large igneous province. Int. Geol. Rev. 45, 753–766.

Xin, W., Sun, F.Y., Xu, Z.H., Lu, Y.H., Zhang, Y.J., Deng, J.F., Li, J.Y., Zhang, Y.T., Gao, H. C., 2020. Potassic/ultrapotassic intrusions at the southwestern margin of the Yangtze Craton, southwestern China: Petrogenesis and implications for the metal and fluid source of non-arc porphyry Cu–(Mo–Au) deposits. Lithos 352-353, 105294. https://doi.org/10.1016/j.lithos.2019.105294.

Xu, Y.G., Menzies, M.A., Thirlwall, M.F., Xie, G.H., 2001. Exotic lithosphere mantle beneath the western Yangtze craton: Petrogenetic links to Tibet using highly magnesian ultrapotassic rocks. Geology 29, 863–866.

Xu, L.L., Bi, X.W., Hu, R.Z., Zhang, X.C., Su, W.C., Qu, W.J., Hu, Z.C., Tang, Y.Y., 2012. Relationships between porphyry Cu–Mo mineralization in the Jinshajiang–Red River metallogenic belt and tectonic activity: constraints from zircon U–Pb and molybdenite Re–Os geochronology. Ore Geol. Rev. 48, 460–473.

Yu, H.Z., Deng, J., Wang, Q.F., Yang, L., Li, H.J., Wang, X., 2020. Petrogenesis of Paleogene lamprophyres in the Ailaoshan tectonic belt, western Yangtze Craton: Implications for the mantle source of orogenic gold deposits. Ore Geol. Rev. 122, 103507 https://doi.org/10.1016/j.oregeorev.2020.103507.

Zhao, J.H., Zhou, M.F., 2007. Geochemistry of Neoproterozoic mafic intrusions in the Panzhihua district (Sichuan Province, SW China): implications for subduction-related metasomatism in the upper mantle. Precambrian Res. 152, 27–47.

Zhao, Z.D., Mo, X.X., Dilek, Y., Niu, Y.L., DePaolo, D.J., Robinson, P., Zhu, D.C., Sun, C. G., Dong, G.C., Zhou, S., Luo, Z.H., Hou, Z.Q., 2009. Geochemical and Sr–Nd–Pb–O isotopic compositions of the post-collisional ultrapotassic magmatism in SW Tibet: Petrogenesis and implications for India intra-continental subduction beneath southern Tibet. Lithos 113, 190–212.

Zhong, D.L., 2000. Paleotethysides in West Yunnan and Sichuan. Science Press, Beijing, China.

Zhou, J.X., 1999. Geochemistry and Petrogenesis of Igneous Rocks Containing Amphibole and mica: A Case Study of Plate Collision Involving Scotland and Himalayas. Science Press, New York, pp. 41–72.

Zhou, M.F., Ma, Y.X., Yan, D.P., Xia, X.P., Zhao, J.H., Sun, M., 2006. The Yanbian Terrane (Southern Sichuan Province, SW China): a Neoproterozoic arc assemblage in the western margin of the Yangtze Block. Precambrian Res. 144, 19–38.

Zhu, X.P., Mo, X.X., White, N.C., Zhang, B., Sun, M.X., Wang, S.X., Zhao, S.L., Yang, Y., 2013. Petrogenesis and metallogenic setting of the Habo porphyry Cu–(Mo–au) deposit, Yunnan, China. J. Asian Earth Sci. 66, 188–203.

Zindler, A., Hart, S.R., 1986. Chemical geodynamics. Annu. Rev. Earth Planet. Sci. 14, 493–571.